

# Two-loop Jet-Function and Jet-Mass for Top Quarks

Ambar Jain,<sup>1</sup> Ignazio Scimemi,<sup>1,2</sup> and Iain W. Stewart<sup>1</sup>

<sup>1</sup>*Center for Theoretical Physics, Massachusetts Institute of Technology, Cambridge, MA 02139*

<sup>2</sup>*Departamento de Física Teórica II, Universidad Complutense de Madrid, 28040 Madrid, Spain*

We compute the two-loop heavy quark jet-function in the heavy quark limit. This is one of the key ingredients in next-to-next-to-leading order (NNLO) and next-to-next-to-leading-log order (NNLL) computations of the invariant mass distribution of top-jets at a future  $e^+e^-$  collider. The shape of the top invariant mass distribution is affected by large logs which we compute at NNLL order. Exploiting the non-abelian exponentiation theorem, a definition of the top jet-mass is given which is transitive and whose renormalization group evolution is determined by the cusp-anomalous dimension to all orders in perturbation theory. Relations of the jet-mass to the pole,  $\overline{\text{MS}}$ , and 1S masses are presented at two-loop order.

MIT-CTP 3916  
0801.0743 [hep-ph]

arXiv:0801.0743v2 [hep-ph] 16 Jun 2008

## I. INTRODUCTION

We are about to step into the LHC era, opening up a new energy regime for the discovery of physics beyond the standard model. In this era precise measurements of standard model parameters will still be important for disentangling new physics scenarios. A prime example of this is the effect of the mass of the top quark on precision electroweak constraints. The latest Tevatron analyses give  $m_t = 170.9 \pm 1.8 \text{ GeV}$  [1], a measurement at the 1% level. However for a minimal standard model Higgs sector the indirect determination of the Higgs mass  $m_H = 76_{-24}^{+33} \text{ GeV}$  has such a strong sensitivity to the top-mass, that a 2 GeV upward shift in  $m_t$  causes this  $m_H$  central value to shift upward by 15% (with the same upward shift for the 95% CL bound  $m_H < 182 \text{ GeV}$ ) [2]. Such strong sensitivities to  $m_t$  are also a feature of many new physics scenarios, such as supersymmetric extensions of the standard model.

In addition to uncertainties related to the experimental analysis, the top-mass also suffers from a theoretical uncertainty related to the specification of the mass-scheme in which the measurement is being made. Many observables used in measurements of the top quark mass incorporate only lowest order theory results, which does not allow one to distinguish between quark mass schemes. In general quark mass schemes are connected by a perturbative series in the strong coupling, with relations of the form

$$m_t^{\text{schemeA}} = m_t^{\text{schemeB}}(1 + \alpha_s + \alpha_s^2 + \dots), \quad m_t^{\text{schemeA}} = m_t^{\text{schemeB}} + R(\alpha_s + \alpha_s^2 + \dots), \quad (1)$$

where  $R$  is a scheme parameter (examples of schemes with relations of both of these types are discussed in the body of the paper). For high precision measurements of the  $b$ -quark mass [3, 4] a useful class of schemes are the so-called threshold mass-schemes, with examples being the kinetic, 1S, and shape-function schemes [5, 6, 7, 8, 9]. For the  $b$ -quark these schemes are optimized to avoid  $\Lambda_{\text{QCD}}$  sensitivities, while still maintaining a power counting in  $\Lambda_{\text{QCD}}/m_b$  to handle non-perturbative corrections in observables. The pole-mass is not used for precision analyses because of its infrared sensitivity, which introduces an ambiguity  $\delta m_b^{\text{pole}} \sim \Lambda_{\text{QCD}}$  from infrared renormalons [10]. For the top quark the infrared physics is cut off by its width  $\Gamma_t = 1.43 \text{ GeV}$ , since tops decay before they hadronize. However the top pole-mass still suffers from a  $\Lambda_{\text{QCD}}$  infrared renormalon ambiguity [11].

Although we do not know the precise scheme for the top-mass measurement of Ref. [1], we do know that it falls in a category of “top resonance mass schemes”, which differ from  $m_t^{\text{pole}}$  by an amount  $\lesssim \Gamma_t$ . This follows from the fact that top-mass measurements rely on an underlying Breit-Wigner to incorporate the top-width, and only top resonance mass schemes are compatible with a Breit-Wigner line-shape [12]. For these observables using a short distance resonance mass-scheme avoids infrared sensitivity while maintaining a  $\Gamma_t/m_t$  expansion. Examples of top resonance mass schemes include the jet-mass [12] and kinetic-mass [5]. For the top-mass this scheme dependence issue could easily add an additional theoretical uncertainty of  $\lesssim 2 \text{ GeV}$  when the measured top-mass is used in practical applications. To see this, lets say that the mass measurement corresponds to  $m_t^{\text{schemeB}}$ , and that we want to use a result for a resonance mass  $m_t^{\text{schemeA}}$  in an analysis. Since scheme B is not precisely known, the perturbative series introduces an additional uncertainty that we estimate to be of  $\mathcal{O}(\alpha_s^2 m_t)$  or  $\mathcal{O}(\alpha_s R)$  from Eq. (1), leading to the  $\lesssim 2 \text{ GeV}$  theoretical error estimate.

In order to obtain higher precision measurements of the top-mass one needs accurate theoretical predictions for a realistic experimental observable in a definite mass scheme. This has been achieved for  $e^+e^- \rightarrow t\bar{t}$  at threshold [13, 14, 15, 16, 17, 18], where state of the art computations incorporate next-to-next-to-leading-log (NNLL) and next-to-next-to-leading order (NNLO) QCD corrections for the cross-section, as well as subleading lifetime effects. Theoretically the necessary setup is also clear for  $e^+e^- \rightarrow t\bar{t}$  far from threshold, where the center-of-mass energy  $Q^2 \gg m_t^2$  [12, 19]. Here the top quark decay products form well separated collinear jets together with soft-radiation between the jets. A suitable observable is the event-shape cross-section  $d^2\sigma/dM_t^2 dM_{\bar{t}}^2$ . Here  $M_t^2 = (\sum_{i \in a} p_i^\mu)^2$  and  $M_{\bar{t}}^2 = (\sum_{i \in b} p_i^\mu)^2$  are hemisphere invariant masses, and the hemispheres a and b are separated by a plane perpendicular to the thrust axis for each event. The different physics components of  $d^2\sigma/dM_t^2 dM_{\bar{t}}^2$  can be separated by a factorization theorem derived in Ref. [12]

$$\begin{aligned} \frac{d\sigma}{dM_t^2 dM_{\bar{t}}^2} &= \sigma_0 H_Q(Q, \mu_m) H_m\left(m, \frac{Q}{m}, \mu_m, \mu\right) \int d\ell^+ d\ell^- B_+\left(\hat{s}_t - \frac{Q\ell^+}{m}, \Gamma_t, \mu\right) B_-\left(\hat{s}_{\bar{t}} - \frac{Q\ell^-}{m}, \Gamma_t, \mu\right) S(\ell^+, \ell^-, \mu) \\ &+ \mathcal{O}\left(\frac{m\alpha_s(m)}{Q}, \frac{m^2}{Q^2}, \frac{\Gamma_t}{m}, \frac{s_t}{m^2}, \frac{s_{\bar{t}}}{m^2}\right). \end{aligned} \quad (2)$$

In Eq. (2)  $\sigma_0$  is the tree level Born cross section,  $H_Q$  and  $H_m$  are hard-functions which encode the perturbative corrections at the scales  $Q$  and  $m$ , where from now on we use  $m$  for the mass of the top quark. The invariant mass variables  $\hat{s}_t$  and  $\hat{s}_{\bar{t}}$  are defined as

$$\hat{s}_t = \frac{s_t}{m} = \frac{M_t^2 - m^2}{m}, \quad \hat{s}_{\bar{t}} = \frac{s_{\bar{t}}}{m} = \frac{M_{\bar{t}}^2 - m^2}{m}, \quad (3)$$

and the most sensitive region for mass measurements is the peak region where  $\hat{s}_{t,\bar{t}} \lesssim \Gamma_t + Q\Lambda_{\text{QCD}}/m$ . Finally,  $B_{\pm}$  in Eq. (2) are heavy-quark jet functions for the top quark/antiquark, and  $S$  is the soft function describing soft radiation between the jets. Our main focus in this article will be on the functions  $B_{\pm}$ , which are defined in the heavy-quark limit  $m_t \gg \Gamma_t$  using heavy quark effective theory (HQET) [20, 21]. The soft function  $S$  is universal to massless and massive jets and a suitable model can be found in Ref. [22], extending earlier work in Ref. [23]. The factorization theorem in Eq. (2) was derived using soft collinear effective theory (SCET) [24, 25, 26, 27] and effective theory methods for unstable particles [28, 29, 30, 31]. A similar factorization theorem with the soft-function and different jet functions is known to apply for jets initiated by massless quarks [32, 33, 34, 35].

In this paper we carry out the first step towards NNLO and NNLL predictions for the invariant mass spectrum,  $d^2\sigma/dM_t^2 dM_{\bar{t}}^2$ , by computing the top quark jet function at two-loop order. We also carry out the resummation of large logs for this jet function at NNLL order. This translates into a resummation of all the large logs in the cross-section that can modify the invariant mass distribution [12]. On the conceptual side we introduce a definition of the top jet-mass scheme that has a well defined mass anomalous dimension at any order in perturbation theory (unlike definitions based on cutoff moments or peak locations). In this jet-mass scheme we prove that the quark-mass anomalous dimension is completely determined by the cusp anomalous dimension at any order in perturbation theory. As an intermediate step to demonstrating this we show that in position space the heavy quark jet function exponentiates. This follows from the fact that this jet function satisfies the criteria for the non-abelian exponentiation theorem [36, 37].

Because of the simplifying nature of HQET our two-loop computation of the jet function is significantly simpler than a direct two-loop computation of the cross-section. In particular, as we discuss below in sections II and III, even for a finite width and an arbitrary mass scheme the jet function computation can be reduced to the perturbative evaluation of a vacuum matrix element of Wilson lines. For heavy quarks two loop computations are already available for the partonic heavy-quark shape function [38, 39, 40] and heavy-quark fragmentation function [38, 39, 41]. The hadronic versions of these functions that appear in observables are non-perturbative. The hadronic shape function describes the light-cone momentum distribution of b-quarks in a heavy B-meson [42, 43], while the hadronic fragmentation function describes the probability that a b-quark fragments to a B-meson with a particular light-cone momentum fraction [44]. The jet function is fundamentally different since it is defined by a matrix element evaluated between vacuum states, and due to the smearing from the finite top-width can be reliably computed in perturbation theory. We elaborate on similarities and differences below in sections II and III.

Our outline is as follows. In section II we discuss the basic formalism for the top quark jet function, including its renormalization and anomalous dimension. We then give a summary of our two-loop results for the jet function and for the solution of its renormalization group equation, with details relegated to appendices. In section III we determine the Wilson line representation of the jet function and compare it with the shape function and fragmentation function. Then in section IV we work out the implications of the non-abelian exponentiation theorem for the heavy-quark jet function and for the partonic shape-function, including the combined implications of this theorem and the all-orders solution of the renormalization group equation. In section V we discuss possible jet-mass scheme definitions, and present a scheme based on the position space jet function that remains transitive to all orders in perturbation theory. We also give two loop relations of the jet-mass to the pole-mass,  $\overline{\text{MS}}$ -mass, and 1S-mass schemes. Finally, in section VI we present results for the NNLO jet function with NNLL resummation, including numerical analysis. We conclude in section VII.

## II. HEAVY QUARK JET FUNCTION

In this section we describe the basic properties of the heavy-quark jet functions  $B_{\pm}$ . Up to a change of variable  $B_+$  for the top quark and  $B_-$  for the antitop quark are identical by charge conjugation, so we will only refer to the computation of  $B_+$ . To simplify the notation we also drop the subscript, so that  $B = B_+$ . These subscripts  $\pm$  are restored when we simultaneously consider the top and antitop system in the final factorization theorem. We start by reviewing definitions and results for the HQET jet function from Refs. [12, 19].  $B$  is given by the imaginary part of a forward scattering matrix element,

$$B(\hat{s}, \delta m, \Gamma_t, \mu) = \text{Im}[\mathcal{B}(\hat{s}, \delta m, \Gamma_t, \mu)] , \quad (4)$$

where  $\mathcal{B}$  are vacuum matrix elements of a time-ordered product of fields and Wilson lines

$$\mathcal{B}(2v_+ \cdot r, \delta m, \Gamma_t, \mu) = \frac{-i}{4\pi N_c m} \int d^4x e^{ir \cdot x} \langle 0 | T \{ \bar{h}_{v_+}(0) W_n(0) W_n^\dagger(x) h_{v_+}(x) \} | 0 \rangle . \quad (5)$$

Here  $v_+^\mu$  is the velocity of the heavy top quark, and we introduce null-vectors  $n^\mu$  and  $\bar{n}^\mu$  so that we can decompose momenta as  $p^\mu = n^\mu \bar{n} \cdot p / 2 + \bar{n}^\mu n \cdot p / 2 + p_\perp^\mu$ . The vectors satisfy  $v_+^2 = 1$  and  $n^2 = \bar{n}^2 = 0$ . The dot-products of these

vectors encode the boost of the top quarks relative to the center-of-mass frame of the  $e^+e^-$  collision,  $n \cdot v_+ = m/Q$ , and  $\bar{n} \cdot v_+ = Q/m$ . In Eq. (5) the Wilson lines are

$$W_n^\dagger(x) = \text{P exp} \left( ig \int_0^\infty ds \bar{n} \cdot A_n(\bar{n}s + x) \right), \quad W_n(x) = \bar{\text{P exp}} \left( -ig \int_0^\infty ds \bar{n} \cdot A_n(\bar{n}s + x) \right). \quad (6)$$

These Wilson lines make  $\mathcal{B}$  gauge-invariant and encode the residual interactions from the antitop jet. Both the HQET fields  $h_{v_+}$  and the gluon fields in  $W_n$  (which we call  $A_n^\mu$ ) are only sensitive to fluctuations with  $p^2 \ll m^2$ . In the rest-frame of the top quark these are soft-fluctuations, while in the  $e^+e^-$  center-of-mass frame they are ‘‘ultra-collinear’’ along the direction of the energetic top quark. The gluon fields  $A_n^\mu$  have zero-bin subtractions [45] for the region of the soft function  $S$  in Eq. (2) as explained in Appendix B of Ref. [19].

The HQET fields  $h_{v_+}$  have the leading order Lagrangian

$$\mathcal{L}_h = \bar{h}_{v_+} \left( iv_+ \cdot D - \delta m + \frac{i}{2} \Gamma_t \right) h_{v_+}. \quad (7)$$

Here  $\Gamma_t$  is the top quark total width, obtained from matching the top-decay amplitudes in the standard model (or a new physics model) onto HQET at leading order in the electroweak interactions, and at any order in  $\alpha_s$ . This gives the correct description of finite lifetime effects for cross-section in Eq. (2) to  $\mathcal{O}(m^2/Q^2, \Gamma/m)$  in the power counting for separation of the jets from the decay products [12]. The residual mass term  $\delta m$  in Eq. (7) fixes the definition of the top mass  $m$  for the HQET computations [46], where

$$\delta m = m_{pole} - m. \quad (8)$$

For predictions in the peak region consistency with the power counting requires  $\delta m \sim \Gamma_t \sim \hat{s}_t \sim \hat{s}_\bar{t}$  [12], a condition which is true of the jet-mass scheme that we discuss below in section V.

From the definitions in Eqs. (4-5) and the Lagrangian in Eq. (7) one can deduce a series of properties of the jet function. As a first, instead of computing  $B(\hat{s}, \delta m, \Gamma_t, \mu)$  and  $\mathcal{B}(\hat{s}, \delta m, \Gamma_t, \mu)$ , one can consider computing these functions for a (fictitious) top quark having zero width. Furthermore, due to Eq. (7) the  $\hat{s}$  and  $\delta m$  dependence occurs in the combination  $(\hat{s} - 2\delta m)$ , so it is useful to also have a notation for computations done with a zero residual mass term in the Lagrangian. Thus we define

$$\begin{aligned} B(\hat{s}, \delta m, \mu) &\equiv B(\hat{s}, \delta m, 0, \mu), & \mathcal{B}(\hat{s}, \delta m, \mu) &\equiv \mathcal{B}(\hat{s}, \delta m, 0, \mu), \\ B(\hat{s}, \mu) &\equiv B(\hat{s}, 0, 0, \mu), & \mathcal{B}(\hat{s}, \mu) &\equiv \mathcal{B}(\hat{s}, 0, 0, \mu). \end{aligned} \quad (9)$$

These jet functions and vacuum matrix elements are related by

$$B(\hat{s}, \delta m, \mu) = \text{Im}[\mathcal{B}(\hat{s}, \delta m, \mu)], \quad \mathcal{B}(\hat{s}, \mu) = \text{Im}[\mathcal{B}(\hat{s}, \mu)], \quad (10)$$

and  $B(\hat{s}, \mu)$  has support for  $\hat{s} \geq 0$ . The form of the Lagrangian in Eq. (7) implies that having calculated  $\mathcal{B}(\hat{s}, \mu)$  we can include the width and  $\delta m$  terms by simple shifts,

$$\mathcal{B}(\hat{s}, \delta m, \Gamma_t, \mu) = \mathcal{B}(\hat{s} + i\Gamma_t, \delta m, \mu) = \mathcal{B}(\hat{s} - 2\delta m + i\Gamma_t, \mu). \quad (11)$$

As discussed in Ref. [19] the stable and unstable HQET jet functions can also be related with a dispersion relation,

$$B(\hat{s}, \delta m, \Gamma_t, \mu) = \int_{-\infty}^{\infty} d\hat{s}' B(\hat{s} - \hat{s}', \delta m, \mu) \frac{\Gamma_t}{\pi(\hat{s}'^2 + \Gamma_t^2)} = \int_{-\infty}^{\infty} d\hat{s}' B(\hat{s} - \hat{s}' - 2\delta m, \mu) \frac{\Gamma_t}{\pi(\hat{s}'^2 + \Gamma_t^2)}. \quad (12)$$

The width of the top quark acts as an infrared cutoff through this smearing with the Breit-Wigner. Finally we remark that the  $\mu$ -dependence indicated by the last argument of  $B(\hat{s}, \delta m, \Gamma_t, \mu)$  and  $\mathcal{B}(\hat{s}, \delta m, \Gamma_t, \mu)$  is independent of  $\Gamma_t$  and  $\delta m$ . Additional scale dependence may be induced by the choice of mass-scheme, ie. by a parameter  $\delta m = \delta m(\mu)$ . When we consider  $B(\hat{s}_t, \delta m, \Gamma_t, \mu)$  as a function of  $M_t$  this additional  $\mu$ -dependence from  $\delta m$  cancels against that in the mass  $m(\mu)$  in Eq. (3). This cancellation occurs at leading order in the HQET power counting.

We will also find it useful to consider the Fourier transformed jet functions

$$\tilde{B}(y, \delta m, \Gamma_t, \mu) = \int_{-\infty}^{+\infty} d\hat{s} e^{-iy\hat{s}} B(\hat{s}, \delta m, \Gamma_t, \mu), \quad \tilde{B}(y, \delta m, \mu) = \int_{-\infty}^{+\infty} d\hat{s} e^{-iy\hat{s}} B(\hat{s}, \delta m, \mu), \quad (13)$$

where  $y = y - i0$  to ensure convergence as  $\hat{s} \rightarrow \infty$ . In Fourier space the connection between the jet functions computed with zero and non-zero width and residual mass terms becomes particularly simple,

$$\tilde{B}(y, \delta m, \Gamma_t, \mu) = \tilde{B}(y, \delta m, \mu) e^{-|y|\Gamma_t} = \tilde{B}(y, \mu) e^{-2iy\delta m} e^{-|y|\Gamma_t}. \quad (14)$$

This formula is quite interesting, since as we discuss in section IV below, the result for  $\tilde{B}(y, \mu)$  also exponentiates to all orders in perturbation theory.

### A. Renormalization and Anomalous Dimension

We use dimensional regularization with  $d = 4 - 2\epsilon$  and the  $\overline{\text{MS}}$  scheme to renormalize the jet function. The renormalization properties of  $B(\hat{s}, \mu)$  and  $\mathcal{B}(\hat{s}, \mu)$  are the same, so in the following we work with  $\mathcal{B}(\hat{s}, \mu)$  for simplicity. The divergences of loop calculations are removed with  $Z$ -factors, so one can pass from bare to renormalized matrix elements by

$$\mathcal{B}(\hat{s}, \mu) = \int d\hat{s}' Z_B^{-1}(\hat{s} - \hat{s}', \mu) \mathcal{B}^{\text{bare}}(\hat{s}'). \quad (15)$$

This equation can be thought of as the generalization of a  $Z$  matrix which renormalizes a set of operators indexed by  $\hat{s}$ , to the case where  $\hat{s}$  is continuous [24]. Here  $Z_B$  and its inverse satisfy

$$\int d\hat{s}' Z_B^{-1}(\hat{s}'' - \hat{s}', \mu) Z_B(\hat{s}' - \hat{s}, \mu) = \delta(\hat{s}'' - \hat{s}). \quad (16)$$

From the  $\mu$  independence of  $\mathcal{B}^{\text{bare}}$  one obtains the renormalization group equation

$$\mu \frac{d}{d\mu} \mathcal{B}(\hat{s}, \mu) = \int d\hat{s}' \gamma_B(\hat{s} - \hat{s}', \mu) \mathcal{B}(\hat{s}', \mu), \quad (17)$$

where the anomalous dimension is

$$\gamma_B(\hat{s}, \mu) = - \int d\hat{s}' Z_B^{-1}(\hat{s} - \hat{s}', \mu) \mu \frac{d}{d\mu} Z_B(\hat{s}', \mu) = \int d\hat{s}' Z_B(\hat{s} - \hat{s}', \mu) \mu \frac{d}{d\mu} Z_B^{-1}(\hat{s}', \mu). \quad (18)$$

Since  $\gamma_B(\hat{s}, \mu)$  is real we can also simply take the imaginary part of Eq. (17) to obtain the renormalization group equation for  $B(\hat{s}, \mu)$ . In the  $\overline{\text{MS}}$  scheme  $Z_B$  and  $Z_B^{-1}$  have the  $\epsilon$  dependence

$$Z_B(\hat{s}, \mu) = \delta(\hat{s}) + \sum_{k=1}^{\infty} \frac{1}{\epsilon^k} Z^{(k)}(\hat{s}, \mu), \quad Z_B^{-1}(\hat{s}, \mu) = \delta(\hat{s}) + \sum_{k=1}^{\infty} \frac{1}{\epsilon^k} \bar{Z}^{(k)}(\hat{s}, \mu), \quad (19)$$

where  $Z^{(k)}$  and  $\bar{Z}^{(k)}$  are  $\epsilon$  independent. Eq. (16) implies that  $\bar{Z}^{(1)} = -Z^{(1)}$ , and  $\bar{Z}^{(k)} = -Z^{(k)} - \sum_{j=1}^{k-1} \bar{Z}^{(j)} \otimes Z^{(k-j)}$  for  $k \geq 2$ . Demanding that  $\gamma_B(\hat{s}, \mu)$  is finite as  $\epsilon \rightarrow 0$  and using the  $\beta$ -function equation

$$\mu \frac{d}{d\mu} \alpha_s(\mu) = -2\epsilon \alpha_s(\mu) + \beta[\alpha_s], \quad (20)$$

gives the standard dimensional regularization result that the anomalous dimension is determined by the residue of the  $1/\epsilon$  term at any order in perturbation theory,

$$\gamma_B(\hat{s}, \mu) = -2\alpha_s \frac{\partial}{\partial \alpha_s} \bar{Z}^{(1)}(\hat{s}, \mu) = 2\alpha_s \frac{\partial}{\partial \alpha_s} Z^{(1)}(\hat{s}, \mu). \quad (21)$$

We find that the higher  $1/\epsilon$  poles lead to the consistency equations [ $\ell \geq 1$ ]

$$2\alpha_s \frac{\partial}{\partial \alpha_s} Z_B^{(\ell+1)}(\hat{s}, \mu) = \left( \mu \frac{\partial}{\partial \mu} + \beta \frac{\partial}{\partial \alpha_s} \right) Z_B^{(\ell)}(\hat{s}, \mu) + \sum_{k=1}^{\ell} \int d\hat{s}' \bar{Z}_B^{(k)}(\hat{s} - \hat{s}', \mu) \left[ -2\alpha_s \frac{\partial}{\partial \alpha_s} Z_B^{(\ell-k+1)}(\hat{s}', \mu) + \left( \mu \frac{\partial}{\partial \mu} + \beta \frac{\partial}{\partial \alpha_s} \right) Z_B^{(\ell-k)}(\hat{s}', \mu) \right], \quad (22)$$

where for convenience we let  $Z_B^{(0)}(\hat{s}, \mu) = \delta(\hat{s})$ . The result in Eq. (22) agrees with the form of the counterterm consistency condition derived in Ref. [40] for the heavy-quark shape function.

At any order in perturbation theory the anomalous dimension in Eq. (21) has the form

$$\gamma_B(\hat{s}, \mu) = -2\Gamma^c[\alpha_s] \frac{1}{\mu} \left[ \frac{\mu \theta(\hat{s})}{\hat{s}} \right]_+ + \gamma[\alpha_s] \delta(\hat{s}), \quad (23)$$

where our definition of this plus-function is given below in Eq. (40). Here  $\Gamma^c[\alpha_s]$  and  $\gamma[\alpha_s]$  have an infinite power series expansions in  $\alpha_s$  that starts at linear order.  $\Gamma^c[\alpha_s]$  is the cusp-anomalous dimension [47, 48, 49, 50], while  $\gamma[\alpha_s]$

is the part of the anomalous dimension that is unrelated to the cusp. In position space the renormalization group equation and anomalous dimension are simpler,

$$\mu \frac{d}{d\mu} \tilde{B}(y, \mu) = \tilde{\gamma}_B(y, \mu) \tilde{B}(y, \mu), \quad \tilde{\gamma}_B(y, \mu) = 2\Gamma^c[\alpha_s] \ln(ie^{\gamma_E} y \mu) + \gamma[\alpha_s]. \quad (24)$$

The form of the anomalous dimensions given in Eqs. (23) and (24) is guaranteed to all orders in perturbation theory by a theorem regarding the renormalization of Wilson-line operators with cusps proven in Ref. [49, 50], which ensures it can not have dependence on the position space variable other than the  $\ln(y\mu)$ . To solve Eq. (24) one first writes  $\ln(ie^{\gamma_E} y \mu) = \ln(ie^{\gamma_E} y \mu_0) + \ln(\mu/\mu_0)$ , then rewrites  $\ln(\mu/\mu_0) = \int_{\alpha_s(\mu_0)}^{\alpha_s(\mu)} d\alpha'/\beta[\alpha']$ , and finally integrates with a change of variables  $d \ln \mu = d\alpha/\beta[\alpha]$ . This gives a solution that connects the result at the scale  $\mu_0$  to that at the scale  $\mu$ ,

$$\tilde{B}(y, \mu) = e^{K(\mu, \mu_0)} (ie^{\gamma_E} y \mu_0)^{\omega(\mu, \mu_0)} \tilde{B}(y, \mu_0), \quad (25)$$

where the two evolution functions are

$$\omega(\mu, \mu_0) = 2 \int_{\alpha_s(\mu_0)}^{\alpha_s(\mu)} \frac{d\alpha}{\beta[\alpha]} \Gamma^c[\alpha], \quad K(\mu, \mu_0) = \int_{\alpha_s(\mu_0)}^{\alpha_s(\mu)} \frac{d\alpha}{\beta[\alpha]} \gamma[\alpha] + 2 \int_{\alpha_s(\mu_0)}^{\alpha_s(\mu)} \frac{d\alpha}{\beta[\alpha]} \Gamma^c[\alpha] \int_{\alpha_s(\mu_0)}^{\alpha} \frac{d\alpha'}{\beta[\alpha']}. \quad (26)$$

Taking the Fourier transform of Eq. (25) then gives the solution to the momentum space renormalization group evolution (RGE) equation

$$B(\hat{s}, \mu) = \int_{-\infty}^{+\infty} d\hat{s}' U_B(\hat{s} - \hat{s}', \mu, \mu_0) B(\hat{s}', \mu_0), \quad U_B(\hat{s} - \hat{s}', \mu, \mu_0) = \frac{e^K (e^{\gamma_E})^\omega}{\mu_0 \Gamma(-\omega)} \left[ \frac{\mu_0^{1+\omega} \theta(\hat{s} - \hat{s}')}{(\hat{s} - \hat{s}')^{1+\omega}} \right]_+, \quad (27)$$

where  $K = K(\mu, \mu_0)$  and  $\omega = \omega(\mu, \mu_0)$ . All results in this subsection are valid to all orders in the  $\alpha_s$  expansion, and can thus be used to sum logs in  $B$  at leading log (LL), next-to-leading log (NLL), NNLL, and beyond. To our knowledge, the results in Eq. (26) and (27) were first derived for the  $B$ -meson shape function, first at one-loop in Ref. [51] and then to all-orders in Ref. [52].

## B. NNLO Result for $\mathcal{B}(\hat{s}, \mu)$

To obtain results at NNLO we consider the  $\alpha_s$  expansion of quantities defined in subsection II A. The bare and renormalized jet functions can be written as

$$\mathcal{B}^{\text{bare}}(\hat{s}) = \sum_{j=0}^{\infty} \left[ \frac{\alpha_s^{\text{bare}}}{\pi} \right]^j \mathcal{B}_j^{\text{bare}}(\hat{s}), \quad \mathcal{B}(\hat{s}, \mu) = \sum_{j=0}^{\infty} \left[ \frac{\alpha_s(\mu)}{\pi} \right]^j \mathcal{B}_j(\hat{s}, \mu). \quad (28)$$

We also expand the anomalous dimensions and  $\beta$ -function as

$$\Gamma^c[\alpha_s] = \sum_{j=0}^{\infty} \Gamma_j^c \left[ \frac{\alpha_s(\mu)}{4\pi} \right]^{j+1}, \quad \gamma[\alpha_s] = \sum_{j=0}^{\infty} \gamma_j \left[ \frac{\alpha_s(\mu)}{4\pi} \right]^{j+1}, \quad \beta[\alpha_s] = -2\alpha_s(\mu) \sum_{n=0}^{\infty} \beta_n \left[ \frac{\alpha_s(\mu)}{4\pi} \right]^{n+1}, \quad (29)$$

where up to three-loop order [53, 54, 55, 56, 57, 58]

$$\begin{aligned} \beta_0 &= \frac{11C_A}{3} - \frac{2n_f}{3}, & \beta_1 &= \frac{34C_A^2}{3} - \frac{10C_A n_f}{3} - 2C_F n_f, \\ \beta_2 &= \frac{2857C_A^3}{54} + \left( C_F^2 - \frac{205C_F C_A}{18} - \frac{1415C_A^2}{54} \right) n_f + \left( \frac{11C_F}{9} + \frac{79C_A}{54} \right) n_f^2. \end{aligned} \quad (30)$$

To incorporate the  $\delta m$  term from the Lagrangian in Eq. (7) we evaluate  $\mathcal{B}_j^{\text{bare}}(\hat{s} - 2\delta m)$  and then expand in  $\alpha_s(\mu)$  with

$$\delta m = \sum_{j=1}^{\infty} \left[ \frac{\alpha_s(\mu)}{\pi} \right]^j \delta m_j(\mu) = \frac{\alpha_s(\mu)}{\pi} \delta m_1(\mu) + \frac{\alpha_s^2(\mu)}{\pi^2} \delta m_2(\mu) + \dots \quad (31)$$

This is simpler than treating  $\delta m$  as a Feynman rule insertion, and equivalent. The bare and renormalized couplings are related by

$$\alpha_s^{\text{bare}} = \iota^\epsilon \mu^{2\epsilon} \alpha_s(\mu) Z_g^2, \quad \iota \equiv \exp(\gamma_E)/(4\pi), \quad (32)$$

where  $Z_g$  is the  $Z$ -factor for the strong coupling and the  $\iota$  dependence,  $\iota^\epsilon$ , ensures we are in the  $\overline{\text{MS}}$  scheme rather than the MS scheme. To determine the renormalized jet function we expand the counterterms as

$$\begin{aligned} Z_B^{-1}(\hat{s}, \mu) &= \delta(\hat{s}) + \sum_{j=1}^{\infty} \left[ \frac{\alpha_s(\mu)}{\pi} \right]^j \bar{Z}_j(\hat{s}, \mu) = \delta(\hat{s}) + \sum_{k=1}^{\infty} \sum_{j=1}^{\infty} \frac{1}{\epsilon^k} \left[ \frac{\alpha_s(\mu)}{\pi} \right]^j \bar{Z}_j^{(k)}(\hat{s}, \mu), \\ Z_g &= 1 + \sum_{j=1}^{\infty} \left[ \frac{\alpha_s(\mu)}{\pi} \right]^j z_{gj}. \end{aligned} \quad (33)$$

Using this notation, converting  $\alpha_s^{\text{bare}}$  to  $\alpha_s(\mu)$  with Eq. (32), and then equating powers of  $\alpha_s(\mu)$  in Eq. (15) these expansions determine the renormalized  $\mathcal{B}_j(\hat{s}, \delta m, \mu)$ . The tree, one-loop, and two-loop coefficients are respectively,

$$\begin{aligned} \mathcal{B}_0(\hat{s}, \delta m, \mu) &= \mathcal{B}_0^{\text{bare}}(\hat{s}), \\ \mathcal{B}_1(\hat{s}, \delta m, \mu) &= \iota^\epsilon \mu^{2\epsilon} \mathcal{B}_1^{\text{bare}}(\hat{s}) + \int d\hat{s}' \bar{Z}_1(\hat{s}-\hat{s}', \mu) \mathcal{B}_0^{\text{bare}}(\hat{s}') - 2\delta m_1 \frac{d\mathcal{B}_0(\hat{s}, \mu)}{d\hat{s}}, \\ \mathcal{B}_2(\hat{s}, \delta m, \mu) &= \iota^{2\epsilon} \mu^{4\epsilon} \mathcal{B}_2^{\text{bare}}(\hat{s}) + 2z_{g1} \iota^\epsilon \mu^{2\epsilon} \mathcal{B}_1^{\text{bare}}(\hat{s}) + \int d\hat{s}' \bar{Z}_1(\hat{s}-\hat{s}', \mu) \iota^\epsilon \mu^{2\epsilon} \mathcal{B}_1^{\text{bare}}(\hat{s}') + \int d\hat{s}' \bar{Z}_2(\hat{s}-\hat{s}', \mu) \mathcal{B}_0^{\text{bare}}(\hat{s}') \\ &\quad - 2\delta m_2 \frac{d\mathcal{B}_0(\hat{s}, \mu)}{d\hat{s}} + 2(\delta m_1)^2 \frac{d^2 \mathcal{B}_0(\hat{s}, \mu)}{d^2 \hat{s}} - 2\delta m_1 \frac{d\mathcal{B}_1(\hat{s}, \mu)}{d\hat{s}}, \end{aligned} \quad (34)$$

where we used a subscript notation for the  $[\alpha_s(\mu)/\pi]^j$  expansion coefficients as in Eq. (28). The one and two-loop  $Z$ -factors have terms

$$\bar{Z}_1 = \frac{1}{\epsilon} \bar{Z}_1^{(1)} + \frac{1}{\epsilon^2} \bar{Z}_1^{(2)}, \quad \bar{Z}_2 = \frac{1}{\epsilon} \bar{Z}_2^{(1)} + \frac{1}{\epsilon^2} \bar{Z}_2^{(2)} + \frac{1}{\epsilon^3} \bar{Z}_2^{(3)} + \frac{1}{\epsilon^4} \bar{Z}_2^{(4)}, \quad (35)$$

where the coefficients  $\bar{Z}_j^{(k)}$  are defined so that the  $\mathcal{B}_j(\hat{s}, \delta m, \mu)$  are finite as  $\epsilon \rightarrow 0$ .

The results for  $\mathcal{B}_0$  and  $\mathcal{B}_1$  were obtained in Ref. [12, 19]. In an arbitrary mass-scheme we have

$$m \mathcal{B}_0(\hat{s}, \delta m, \mu) = L^0, \quad m \mathcal{B}_1(\hat{s}, \delta m, \mu) = C_F \left\{ L^2 + L^1 + \left( 1 + \frac{5\pi^2}{24} \right) L^0 \right\} - 2\delta m_1 (L^0)', \quad (36)$$

where the prime denotes a derivative with respect to  $\hat{s}$ , and for convenience we have defined

$$L^k = \frac{1}{\pi(-\hat{s}-i0)} \ln^k \left( \frac{\mu}{-\hat{s}-i0} \right). \quad (37)$$

The corresponding two-loop result,  $\mathcal{B}_2$ , is one of the main results of this paper and involves the Feynman diagrams shown in Fig. 1. Details of the computation of  $\mathcal{B}_2$  using Eq. (34) in Feynman gauge are given in Appendix A. To summarize, we use the computation of Broadhurst and Grozin [59, 60] for the divergent and finite terms of the two-loop heavy quark propagator (the first graph in Fig. 1), and compute the remaining Feynman diagrams directly. We treat the quarks other than top as massless, with  $n_f$  such flavors, and thus do not include effects due to the  $b$ -quark mass in vacuum polarization diagrams. We have also confirmed that the resulting  $\bar{Z}_j^{(k)}$  satisfy the counterterm consistency conditions in Eq. (22). The final result for the renormalized two-loop matrix element is

$$\begin{aligned} m \mathcal{B}_2(\hat{s}, \delta m, \mu) &= C_F^2 \left[ \frac{1}{2} L^4 + L^3 + \left( \frac{3}{2} + \frac{13\pi^2}{24} \right) L^2 + \left( 1 + \frac{13\pi^2}{24} - 4\zeta_3 \right) L^1 + \left( \frac{1}{2} + \frac{7\pi^2}{24} + \frac{53\pi^4}{640} - 2\zeta_3 \right) L^0 \right] \\ &\quad + C_F C_A \left[ \left( \frac{1}{3} - \frac{\pi^2}{12} \right) L^2 + \left( \frac{5}{18} - \frac{\pi^2}{12} - \frac{5\zeta_3}{4} \right) L^1 + \left( -\frac{11}{54} + \frac{5\pi^2}{48} - \frac{19\pi^4}{960} - \frac{5\zeta_3}{8} \right) L^0 \right] \\ &\quad + C_F \beta_0 \left[ \frac{1}{6} L^3 + \frac{2}{3} L^2 + \left( \frac{47}{36} + \frac{\pi^2}{12} \right) L^1 + \left( \frac{281}{216} + \frac{23\pi^2}{192} - \frac{17\zeta_3}{48} \right) L^0 \right] \\ &\quad - 2\delta m_2 (L^0)' + 2(\delta m_1)^2 (L^0)'' - 2\delta m_1 C_F \left[ L^2 + L^1 + \left( 1 + \frac{5\pi^2}{24} \right) L^0 \right]'. \end{aligned} \quad (38)$$

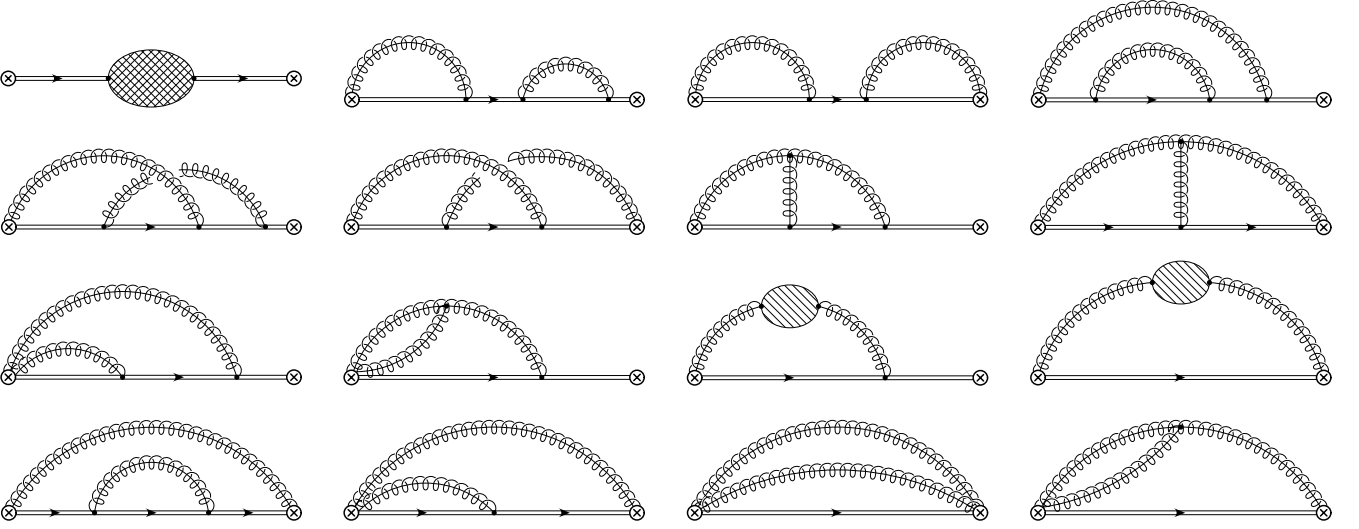


FIG. 1: Graphs for  $\mathcal{B}_2^{\text{bare}}(\hat{s})$ . Gluons from an  $\otimes$  are from the Wilson lines, the hatched blob is the two-loop vacuum polarization of the heavy quark, and the blobs with diagonal lines include all one-loop vacuum polarization graphs for the gluon. Numbering the graphs from 1 to 16 from left-to-right and top-to-bottom, we note that graphs 2, 4, 5, 7, 9, 10, 11, 14, and 16 implicitly also stand for their left-right symmetric counterpart.

One can pass from the function  $\mathcal{B}(\hat{s}, \delta m, \mu)$  to the distribution  $B(\hat{s}, \delta m, \mu)$  using Eq. (10) and the formulas in Eq. (B3). This gives

$$\begin{aligned}
m B(\hat{s}, \delta m, \mu) = & \delta(\hat{s}) + \frac{C_F \alpha_s(\mu)}{\pi} \left\{ 2\mathcal{L}^1 - \mathcal{L}^0 + \left(1 - \frac{\pi^2}{8}\right) \delta(\hat{s}) \right\} - \frac{2\alpha_s(\mu)}{\pi} \delta m_1(\mu) \delta'(\hat{s}) \\
& + \frac{\alpha_s^2(\mu)}{\pi^2} \left\{ C_F^2 \left[ 2\mathcal{L}^3 - 3\mathcal{L}^2 + \left(3 - \frac{11\pi^2}{12}\right) \mathcal{L}^1 + \left(-1 + \frac{11\pi^2}{24} + 4\zeta_3\right) \mathcal{L}^0 + \left(\frac{1}{2} - \frac{5\pi^2}{24} + \frac{13\pi^4}{5760} - 2\zeta_3\right) \delta(\hat{s}) \right] \right. \\
& + C_F C_A \left[ \left(\frac{2}{3} - \frac{\pi^2}{6}\right) \mathcal{L}^1 + \left(-\frac{5}{18} + \frac{\pi^2}{12} + \frac{5\zeta_3}{4}\right) \mathcal{L}^0 + \left(-\frac{11}{54} - \frac{\pi^2}{144} + \frac{23\pi^4}{2880} - \frac{5\zeta_3}{8}\right) \delta(\hat{s}) \right] \\
& + C_F \beta_0 \left[ -\frac{1}{2} \mathcal{L}^2 + \frac{4}{3} \mathcal{L}^1 + \left(-\frac{47}{36} + \frac{\pi^2}{12}\right) \mathcal{L}^0 + \left(\frac{281}{216} - \frac{59\pi^2}{576} - \frac{17\zeta_3}{48}\right) \delta(\hat{s}) \right] \left. \right\} \\
& - \frac{2\alpha_s^2(\mu)}{\pi^2} \left\{ \delta m_2 \delta'(\hat{s}) - (\delta m_1)^2 \delta''(\hat{s}) + \delta m_1 C_F \left[ 2(\mathcal{L}^1)' - (\mathcal{L}^0)' + \left(1 - \frac{\pi^2}{8}\right) \delta'(\hat{s}) \right] \right\}, \tag{39}
\end{aligned}$$

where for the log plus-functions we use the notation

$$\mathcal{L}^k = \frac{1}{\mu} \left[ \frac{\theta(\hat{s}) \ln^k(\hat{s}/\mu)}{\hat{s}/\mu} \right]_+ \equiv \lim_{\xi \rightarrow 0} \frac{1}{\mu} \left[ \frac{\theta(x-\xi) \ln^k x}{x} + \delta(x-\xi) \frac{\ln^{k+1} \xi}{k+1} \right]_{x=\hat{s}/\mu}. \tag{40}$$

The results in Eqs. (38) and (39) are presented in an arbitrary mass scheme, which is specified by the choice for the coefficients  $\delta m_1$  and  $\delta m_2$ . An appropriate mass-scheme for top-jet cross sections is described below in section V. In order to obtain the distribution  $B(\hat{s}, \delta m, \Gamma_t, \mu)$  with  $\Gamma_t \neq 0$  one can input Eq. (39) into the integral with the Breit-Wigner in Eq. (12). However the simpler method, which we use below in section VI, is to shift  $\hat{s} \rightarrow \hat{s} + i\Gamma_t$  in Eqs. (36,38) and then take the imaginary part as in Eq. (11).

From the renormalization constants  $Z_1^{(1)}$  and  $Z_2^{(1)}$  given in Appendix A we also obtain the anomalous dimension terms in Eq. (29). The cusp anomalous dimension is known up to three-loop order  $\Gamma_{0,1,2}^c$  [50, 61], and we have confirmed that our two-loop analysis reproduces the expected result for the two-loop cusp coefficient,  $\Gamma_1^c$ . For  $\mathcal{B}$  the one-loop anomalous dimension  $\gamma_0$  has been calculated in Ref. [19]. The two-loop anomalous dimension  $\gamma_1$  is obtained



from our calculation of  $\bar{Z}_2^{(1)}$  in Eq. (A11).<sup>1</sup> We list here all the pieces needed for our analysis,

$$\begin{aligned}\Gamma_0^c &= 4C_F, & \Gamma_1^c &= \left(\frac{268}{9} - \frac{4\pi^2}{3}\right)C_F C_A - \frac{40}{9}C_F n_f, \\ \Gamma_2^c &= \left[\frac{490}{3} - \frac{536\pi^2}{27} + \frac{44\pi^4}{45} + \frac{88\zeta_3}{3}\right]C_F C_A^2 + \left[\frac{80\pi^2 - 836}{27} - \frac{112\zeta_3}{3}\right]C_F n_f C_A + \left[32\zeta_3 - \frac{110}{3}\right]C_F^2 n_f - \frac{16C_F n_f^2}{27}, \\ \gamma_0 &= 4C_F, & \gamma_1 &= \left[\frac{1396}{27} - \frac{23\pi^2}{9} - 20\zeta_3\right]C_F C_A + \left[\frac{2\pi^2}{9} - \frac{232}{27}\right]C_F n_f.\end{aligned}\quad (41)$$

To resum the large logs in the jet function to NNLL order we need to use these coefficients in the NNLL results for the evolution functions  $\omega(\mu, \mu_0)$  and  $K(\mu, \mu_0)$ . To NNLL order solving Eq. (26) gives

$$\begin{aligned}\omega(\mu, \mu_0) &= -\frac{\Gamma_0^c}{\beta_0} \left\{ \ln(r) + \left(\frac{\Gamma_1^c}{\Gamma_0^c} - \frac{\beta_1}{\beta_0}\right) \frac{\alpha_s(\mu_0)}{4\pi} (r-1) + \left(\frac{\Gamma_2^c}{\Gamma_0^c} - \frac{\beta_1\Gamma_1^c}{\beta_0\Gamma_0^c} - \frac{\beta_2}{\beta_0} + \frac{\beta_1^2}{\beta_0^2}\right) \frac{\alpha_s^2(\mu_0)}{32\pi^2} (r^2-1) \right\}, \\ K(\mu, \mu_0) &= \frac{-2\pi\Gamma_0^c}{\beta_0^2} \left\{ \frac{(r-1-r\ln r)}{r\alpha_s(\mu_0)} + \frac{\gamma_0\beta_0}{4\pi\Gamma_0^c} \ln r + \left(\frac{\Gamma_1^c}{\Gamma_0^c} - \frac{\beta_1}{\beta_0}\right) \frac{(1-r+\ln r)}{4\pi} + \frac{\beta_1}{8\pi\beta_0} \ln^2 r + \frac{\alpha_s(\mu_0)}{16\pi^2} \left[ \frac{(\beta_0\gamma_1 - \beta_1\gamma_0)}{\Gamma_0^c} (r-1) \right. \right. \\ &\quad \left. \left. + \left(\frac{\beta_1\Gamma_1^c}{\beta_0\Gamma_0^c} - \frac{\beta_2}{\beta_0}\right) (1-r+r\ln r) + \left(\frac{\beta_2}{\beta_0} - \frac{\beta_1^2}{\beta_0^2}\right) (r-1) \ln r - \left(\frac{\Gamma_2^c}{\Gamma_0^c} - \frac{\beta_1\Gamma_1^c}{\beta_0\Gamma_0^c} - \frac{\beta_2}{\beta_0} + \frac{\beta_1^2}{\beta_0^2}\right) \frac{(1-r)^2}{2} \right] \right\},\end{aligned}\quad (42)$$

where  $r = \alpha_s(\mu)/\alpha_s(\mu_0)$ . Eq. (42) determines the evolution functions in terms of coefficients of the anomalous dimensions and  $\beta$ -function. It agrees with the NNLL result given in the appendix of Ref. [52], which was used to sum large logs in the  $B$ -meson shape function for  $B \rightarrow X_s\gamma$ .

We postpone presenting our final resummed NNLL result for the jet function until section VI.

### III. WILSON LOOP REPRESENTATIONS, AND COMPARISON WITH THE HEAVY QUARK SHAPE FUNCTION AND FRAGMENTATION FUNCTION

It is well known that the leading order coupling of gluons to heavy-quark fields  $h_v$  in HQET can be represented by Wilson lines along the path of the heavy-quark [62]. We define

$$W_v(x) = \bar{P} \exp \left( -ig \int_0^\infty ds v \cdot A(vs+x) \right), \quad W_v^\dagger(x) = P \exp \left( ig \int_0^\infty ds v \cdot A(vs+x) \right). \quad (43)$$

To see how the HQET action reduces to a Wilson line one can make a field redefinition,  $h_v = W_v h_v^{(0)}$ , from which we find that  $h_v^{(0)}$  is a free field with Lagrangian  $\mathcal{L}_h = \bar{h}_v^{(0)} i v \cdot \partial h_v^{(0)}$ , see [26]. Thus, the vacuum matrix element for the heavy-quark jet function in Eq. (5) can be written as a matrix element of Wilson lines

$$\begin{aligned}\mathcal{B}(2v \cdot r, \mu) &= \frac{-i}{4\pi N_c m} \int d^4x e^{ir \cdot x} \langle 0 | T \bar{h}_v^{(0)}(0) W_v^\dagger(0) W_n(0) W_n^\dagger(x) W_v(x) h_v^{(0)}(x) | 0 \rangle \\ &= \frac{i}{2\pi N_c m} \int dx^0 e^{iv \cdot r x^0} \theta(x^0) \langle 0 | \text{tr} T W_v^\dagger(0) W_n(0) W_n^\dagger(x^0) W_v(x^0) | 0 \rangle \\ &= \frac{i}{2\pi N_c m} \int dx^0 e^{iv \cdot r x^0} \theta(x^0) \langle 0 | \text{tr} T W_v(x^0, 0) W_n(0, \infty, x^0) | 0 \rangle,\end{aligned}\quad (44)$$

where  $2v \cdot r = \hat{s}$  and we use the shorthand  $x^0 = v \cdot x$ , the trace tr is over color indices. Here  $W_v(x^0, 0) = W_v(x^0) W_v^\dagger(0)$  is the straight Wilson line from 0 to  $x^0$ , while  $W_n(0, \infty, x^0) \equiv W_n(0) W_n^\dagger(x^0)$  has a path from  $x^0$  to  $\infty$  to 0 that uses two light-like line-segments. To obtain the second line of Eq. (44) we used the heavy-quark propagator,  $\langle 0 | T \bar{h}_v^{(0)a}(0) h_v^{(0)b}(x) | 0 \rangle = -2\delta^{ab} \delta^3(\vec{x}) \theta(x^0)$  where  $a$  and  $b$  are color indices. In Fig. 2a we give a graphical representation for the Wilson line definition in the last line of Eq. (44). The arrows denote the time-ordering.

<sup>1</sup> It turns out that the piece of  $\gamma_1$  proportional to  $C_F n_f$  is the analog of a contribution in the analysis of a scalar field theory made in Ref. [29, 30]. Suitably translated to the QCD case their computation agrees with the  $C_F n_f$  term in our  $\gamma_1$ . The non-abelian  $C_F C_A$  term of  $\gamma_1$  is original to our work.

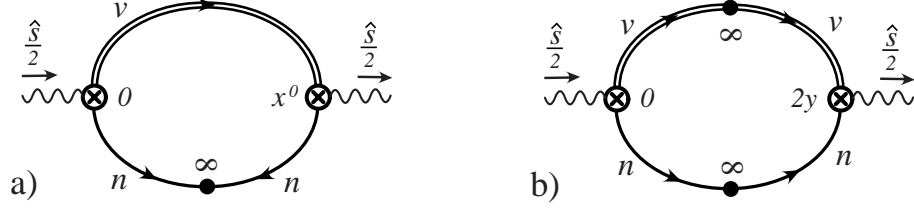


FIG. 2: Representations of the Wilson line matrix elements for the heavy quark jet function, The Wilson lines include  $W_v$ ,  $W_v^\dagger$  (double lines), and  $W_n$ ,  $W_n^\dagger$  (single lines). In a) we display the result in Eq. (44) that gives  $\mathcal{B}(\hat{s}, \mu)$ . In b) we display the result in Eq. (46) that gives  $B(\hat{s}, \mu)$ .

We can also write the jet function  $B(\hat{s}, \mu)$  as a matrix element of Wilson lines. To derive this result we note that

$$\begin{aligned}
 B(2v \cdot r, \mu) &= \frac{1}{8\pi N_c m} \int d^4x e^{ir \cdot x} \sum_X \text{Tr} \langle 0 | \bar{T} W_n^\dagger(x) h_v(x) | X \rangle \langle X | T \bar{h}_v(0) W_n(0) | 0 \rangle \\
 &= \frac{1}{8\pi N_c m} \int d^4x e^{ir \cdot x} \text{Tr} \langle 0 | [ \bar{T} W_n^\dagger(x) h_v(x) ] [ T \bar{h}_v(0) W_n(0) ] | 0 \rangle \\
 &= \frac{1}{8\pi N_c m} \int d^4x e^{ir \cdot x} \text{Tr} \langle 0 | [ \bar{T} W_n^\dagger(x) W_v(x) h_v^{(0)}(x) ] [ T \bar{h}_v^{(0)}(0) W_v^\dagger(0) W_n(0) ] | 0 \rangle, \quad (45)
 \end{aligned}$$

where  $T$  is time-ordering,  $\bar{T}$  is anti-time-ordering, and the trace  $\text{Tr}$  is over spin and color indices. Next we use  $\langle 0 | h_{vi}^{(0)a}(x) \bar{h}_{vi}^{(0)b}(0) | 0 \rangle = 2\delta^{ab} \delta^3(\vec{x})$ , where here there is no time-ordering and hence no  $\theta(x^0)$ , and the spin indices  $i$  are contracted. Thus

$$B(\hat{s}, \mu) = \frac{1}{2\pi} \int dy e^{is y} \tilde{B}(y, \mu), \quad \tilde{B}(y, \mu) = \frac{1}{m N_c} \langle 0 | \text{tr} [ \bar{T} W_n^\dagger(2y) W_v(2y) ] [ T W_v^\dagger(0) W_n(0) ] | 0 \rangle. \quad (46)$$

Here we took  $x^0 = 2y$  in order to agree with the notation for the position space jet function  $\tilde{B}(y, \mu)$  above in Eq. (13). In Fig. 2b we give a graphical representation for the Wilson line matrix element for  $B(\hat{s}, \mu)$  in Eq. (46), where the arrows denote the time-ordering. Comparing to the Wilson loop for  $\mathcal{B}(\hat{s}, \mu)$  in Fig. 2a we note the importance of the  $\infty$ -points to determine which fields are time-ordered and which are antitime-ordered.

It is instructive to compare the Wilson line definition of the heavy quark jet function with the corresponding definitions for the heavy quark shape function that appears in  $B$ -decays [42, 43], and with the heavy quark fragmentation function [44]. Using a variable  $\ell^+ \geq 0$ , the  $B$ -meson shape function is given by

$$\begin{aligned}
 f^{B_v}(\ell^+, \mu) &= \frac{1}{8\pi} \int dx^- e^{-i(\ell^+ - \bar{\Lambda})x^- / 2} \sum_X \langle \bar{B}_v | \bar{T} \bar{h}_v(0) W_n(0) | X \rangle \langle X | T W_n^\dagger(\tilde{x}) h_v(\tilde{x}) | \bar{B}_v \rangle \\
 &= \frac{1}{8\pi} \int dx^- e^{-i(\ell^+ - \bar{\Lambda})x^- / 2} \langle \bar{B}_v | [ \bar{T} \bar{h}_v^{(0)}(0) \tilde{W}_v^\dagger(0) W_n(0) ] [ T W_n^\dagger(\tilde{x}) \tilde{W}_v(\tilde{x}) h_v^{(0)}(\tilde{x}) ] | \bar{B}_v \rangle \\
 &= \frac{1}{8\pi} \int dx^- e^{-i(\ell^+ - \bar{\Lambda})x^- / 2} \langle \bar{B}_v | \bar{h}_v^{(0)}(0) \tilde{W}_v^\dagger(0) W_n(0, \tilde{x}) \tilde{W}_v(\tilde{x}) h_v^{(0)}(\tilde{x}) | \bar{B}_v \rangle, \quad (47)
 \end{aligned}$$

where we use the shorthand  $x^- = \bar{n} \cdot x$  and  $\tilde{x}^\mu = x^- n^\mu / 2$ , and set  $\bar{n} \cdot v = 1$ . To obtain the second line we made the same field redefinition as above in Eq. (43), but now on both the heavy-quark field and on the interpolating field for the  $B$ -meson [63, 64]. Combining the lines from these sources yielded the Wilson lines

$$\tilde{W}_v(x) = P \exp \left( ig \int_{-\infty}^0 ds v \cdot A(vs+x) \right), \quad \tilde{W}_v^\dagger(x) = \bar{P} \exp \left( -ig \int_{-\infty}^0 ds v \cdot A(vs+x) \right). \quad (48)$$

To obtain the third line of Eq. (47) we noted that  $T W_n^\dagger = W_n^\dagger$ ,  $\bar{T} W_n = W_n$ ,  $T \tilde{W}_v = \tilde{W}_v$ , and  $\bar{T} \tilde{W}_v^\dagger = \tilde{W}_v^\dagger$ , and that the gluons in the Wilson lines which sit next to each other,  $W_n^\dagger(\tilde{x}) \tilde{W}_v(\tilde{x})$  and  $\tilde{W}_v^\dagger(0) W_n(0)$ , are already time-ordered and anti-time-ordered respectively.

For the  $B$ -meson fragmentation function in HQET with variable  $\ell^+ \geq 0$ , the field redefinition gives

$$\begin{aligned}
 D^{B_v/b}(\ell^+, \mu) &= \frac{1}{16\pi} \int dx^- e^{i(\ell^+ + \bar{\Lambda})x^- / 2} \sum_X \langle 0 | \bar{T} \tilde{W}_n^\dagger(\tilde{x}) h_v(\tilde{x}) | \bar{B}_v X \rangle \langle \bar{B}_v X | T \bar{h}_v(0) \tilde{W}_n(0) | 0 \rangle \\
 &= \frac{1}{16\pi} \int dx^- e^{i(\ell^+ + \bar{\Lambda})x^- / 2} \sum_X \langle 0 | \bar{T} \tilde{W}_n^\dagger(\tilde{x}) W_v(\tilde{x}) h_v^{(0)}(\tilde{x}) | \bar{B}_v X \rangle \langle \bar{B}_v X | T \bar{h}_v^{(0)}(0) W_v^\dagger(0) \tilde{W}_n(0) | 0 \rangle. \quad (49)
 \end{aligned}$$

Here  $\tilde{W}_n$  and  $\tilde{W}_n^\dagger$  are defined as in Eq. (48) but with  $v \rightarrow \bar{n}$ . The shape and fragmentation function results in Eq. (47) and (49) are similar to the heavy-quark jet function in that all three are defined by matrix elements with heavy-quark fields and Wilson lines. They differ because they are non-perturbative distributions involving a  $B$ -meson state in contrast to the perturbatively computable jet function. The shape and fragmentation functions also have a light-cone separation rather than the time-like separation that we have for the jet function.

In certain contexts it is also useful to consider the partonic shape function  $f^{b_v}$  and the partonic fragmentation function  $D^{b_v/b}$  where the  $B_v$ -meson state is replaced by a  $b_v$ -quark with residual momentum  $k^\mu$ , where  $\bar{\Lambda} = 0$ . In this case we can perform the contraction  $h_v^{(0)}(x)|\bar{b}_v\rangle = e^{-ik \cdot x} u_v|0\rangle/\sqrt{N_c}$  and write

$$\begin{aligned} f_{k^+}^{b_v}(\ell^+, \mu) &= \frac{1}{4\pi N_c} \int dx^- e^{-i(\ell^+ + k^+)x^-/2} \langle 0 | \text{tr} \tilde{W}_v^\dagger(0) W_n(0, \tilde{x}) \tilde{W}_v(\tilde{x}) | 0 \rangle, \\ D_{k^+}^{b_v/b}(\ell^+, \mu) &= \frac{1}{4\pi N_c} \int dx^- e^{i(\ell^+ - k^+)x^-/2} \langle 0 | \text{tr} \tilde{W}_n^\dagger(\tilde{x}) W_v(\tilde{x}) W_v^\dagger(0) \tilde{W}_n(0) | 0 \rangle \\ &= \frac{1}{4\pi N_c} \int dx^- e^{i(\ell^+ - k^+)x^-/2} \langle 0 | \text{tr} \tilde{W}_n^\dagger(\tilde{x}) \tilde{W}_v(\tilde{x}) \tilde{W}_v^\dagger(0) \tilde{W}_n(0) | 0 \rangle \\ &= \frac{1}{4\pi N_c} \int dx^- e^{i(\ell^+ - k^+)x^-/2} \langle 0 | \text{tr} \tilde{W}_v^\dagger(0) W_n(0, \tilde{x}) \tilde{W}_v(\tilde{x}) | 0 \rangle \\ &= f_{k^+}^{b_v}(-\ell^+, \mu), \end{aligned} \quad (50)$$

where we used  $\tilde{W}_n(0)\tilde{W}_n^\dagger(\tilde{x}) = W_n(0)W_n^\dagger(\tilde{x}) = W_n(0, \tilde{x})$ . Eq. (50) states that the partonic shape function and fragmentation function are identical, but with complementary ranges of support. This was observed in Ref. [39] for logs at NNLL accuracy, and was derived to all orders in perturbation theory in Ref. [41] as we outlined above. Thus, the partonic shape function in position space,  $\tilde{f}^{b_v}(y, \mu)$  is also given by a vacuum matrix of Wilson lines. It differs from  $\tilde{B}(y, \mu)$  in Eq. (44) both due to the light-like rather than time-like separation  $y = x^-/2$ , and due to the path.

#### IV. NON-ABELIAN EXPONENTIATION

In the previous section in Eq. (46) we showed that the position space heavy-quark jet function  $\tilde{B}(y, \mu)$  is determined by a vacuum matrix element of Wilson lines. Due to the non-abelian exponentiation theorem [36, 37] for matrix elements of Wilson lines with symmetric restrictions on the phase space of real gluons,  $\tilde{B}(y, \mu)$  exponentiates. This is also true of the partonic heavy-quark shape function in position space.

Taking the Fourier transform of the two-loop jet function result in Eq. (39) using Eq. (B1) we obtain

$$\begin{aligned} m\tilde{B}(y, \mu) &= 1 + \frac{C_F \alpha_s(\mu)}{\pi} \left( \tilde{L}^2 + \tilde{L} + \frac{\pi^2}{24} + 1 \right) + \frac{\alpha_s^2(\mu)}{\pi^2} \left\{ C_F \beta_0 \left[ \frac{1}{6} \tilde{L}^3 + \frac{2}{3} \tilde{L}^2 + \frac{47}{36} \tilde{L} - \frac{\zeta_3}{48} + \frac{5\pi^2}{576} + \frac{281}{216} \right] \right. \\ &\quad + C_F C_A \left[ \left( \frac{1}{3} - \frac{\pi^2}{12} \right) \tilde{L}^2 + \left( \frac{5}{18} - \frac{\pi^2}{12} - \frac{5\zeta_3}{4} \right) \tilde{L} - \frac{5\zeta_3}{8} - \frac{17\pi^4}{2880} + \frac{7\pi^2}{144} - \frac{11}{54} \right] \\ &\quad \left. + C_F^2 \left[ \frac{1}{2} \tilde{L}^4 + \tilde{L}^3 + \left( \frac{3}{2} + \frac{\pi^2}{24} \right) \tilde{L}^2 + \left( 1 + \frac{\pi^2}{24} \right) \tilde{L} + \frac{\pi^4}{1152} + \frac{\pi^2}{24} + \frac{1}{2} \right] \right\}, \end{aligned} \quad (51)$$

where  $\tilde{L}^k = (\tilde{L})^k$  and

$$\tilde{L} \equiv \ln(i e^{\gamma_E} y \mu). \quad (52)$$

It is evident in Eq. (51) that the two-loop,  $C_F^2 \alpha_s^2$  term satisfies the exponentiation theorem, being determined by one-half the square of the one-loop  $C_F \alpha_s$  term. Thus we can write

$$\begin{aligned} m\tilde{B}(y, \mu) &= \exp \left\{ \frac{C_F \alpha_s(\mu)}{\pi} \left( \tilde{L}^2 + \tilde{L} + \frac{\pi^2}{24} + 1 \right) + \frac{\alpha_s^2(\mu) C_F \beta_0}{\pi^2} \left[ \frac{1}{6} \tilde{L}^3 + \frac{2}{3} \tilde{L}^2 + \frac{47}{36} \tilde{L} - \frac{\zeta_3}{48} + \frac{5\pi^2}{576} + \frac{281}{216} \right] \right. \\ &\quad \left. + \frac{\alpha_s^2(\mu) C_F C_A}{\pi^2} \left[ \left( \frac{1}{3} - \frac{\pi^2}{12} \right) \tilde{L}^2 + \left( \frac{5}{18} - \frac{\pi^2}{12} - \frac{5\zeta_3}{4} \right) \tilde{L} - \frac{5\zeta_3}{8} - \frac{17\pi^4}{2880} + \frac{7\pi^2}{144} - \frac{11}{54} \right] \right\}. \end{aligned} \quad (53)$$

The non-abelian exponentiation theorem guarantees that corrections to this result are  $\mathcal{O}(\alpha_s^3)$  in the exponent, and that these corrections will vanish if we take the abelian limit  $C_A \rightarrow 0$  and  $n_f \rightarrow 0$ .

In the abelian limit with zero  $\beta$ -function, the exponentiation theorem implies that  $\ln[m\tilde{B}(y, \mu)]$  is one-loop exact. Thus taking  $C_A = n_f = 0$ , and a charge  $C_F$  we have to all orders in perturbation theory

$$m\tilde{B}(y, \mu)^{\text{abelian}} = \exp \left[ \frac{\alpha_s}{4\pi} \left( \Gamma_0^c \tilde{L}^2 + \gamma_0 \tilde{L} + T_0 \right) \right], \quad (54)$$

where the constants are  $\Gamma_0^c = \gamma_0 = 4C_F$  and  $T_0 = 4C_F(1 + \pi^2/24)$ . The exact result in Eq. (54) provides a simple way of testing the properties of different possible jet-mass definitions at higher orders in perturbation theory, as discussed in section V.

We can also consider the implications of the non-abelian exponentiation theorem for the solution of the renormalization group equation (25). Following Ref. [22] we first use the evolution kernel  $K(\mu, \mu_0)$  to solve for  $\tilde{B}(y, \mu)$  by taking  $\mu_0 = \mu_y \equiv -ie^{-\gamma_E}/y$ . This makes all the logs in  $\tilde{B}(y, \mu_y)$  vanish since  $\tilde{L}(\mu_y) = \ln(ie^{\gamma_E}y\mu_y) = 0$ . Thus

$$m\tilde{B}(y, \mu) = e^{K(\mu, \mu_y)} m\tilde{B}(y, \mu_y) = e^{K(\mu, \mu_y) + T[\alpha_s(\mu_y)]}. \quad (55)$$

Here the boundary condition for the RGE, denoted  $m\tilde{B}(y, \mu_y)$ , is just a perturbative series in  $\alpha_s(\mu_y)$ . Due to the non-abelian exponentiation theorem this series must exponentiate to give  $\exp(T[\alpha_s(\mu_y)])$ , and the coefficients in the perturbative series for  $T[\alpha_s]$  have color factors that satisfy the exponentiation theorem constraints. It is a straightforward exercise to verify that expanding the result for  $K(\mu, \mu_0)$  in Eq. (42) to  $\mathcal{O}(\alpha_s^2)$  gives a result from Eq. (55) that is consistent with Eq. (53).

The Fourier transformed partonic b-quark shape function is also given by a vacuum matrix element of Wilson lines via Eq. (50). Thus, it too satisfies the criteria of the non-abelian exponentiation theorem [38]. Taking the Fourier transform of the two-loop computation of  $f^{b_v}(\ell^+, \mu)$  in Ref. [40] we have verified that the  $C_F^2\alpha_s^2$  terms satisfy the non-abelian exponentiation theorem. This calculation gives

$$\begin{aligned} \tilde{f}^{b_v}(y, \mu) = \exp \left\{ \frac{-C_F\alpha_s(\mu)}{\pi} \left( \tilde{L}^2 - \tilde{L} + \frac{5\pi^2}{24} \right) + \frac{\alpha_s^2(\mu)C_F\beta_0}{\pi^2} \left[ -\frac{1}{6}\tilde{L}^3 - \frac{1}{6}\tilde{L}^2 + \frac{(1-3\pi^2)}{36}\tilde{L} - \frac{11\zeta_3}{48} - \frac{7\pi^2}{192} + \frac{1}{216} \right] \right. \\ \left. + \frac{\alpha_s^2(\mu)C_FC_A}{\pi^2} \left[ -\left( \frac{1}{3} - \frac{\pi^2}{12} \right) \tilde{L}^2 + \left( -\frac{11}{18} - \frac{\pi^2}{12} + \frac{9\zeta_3}{4} \right) \tilde{L} - \frac{9\zeta_3}{8} + \frac{107\pi^4}{2880} - \frac{13\pi^2}{48} - \frac{29}{108} \right] \right\}, \quad (56) \end{aligned}$$

where  $\tilde{L}$  is defined in Eq. (52), but now  $y$  is the conjugate variable to  $\ell^+$ ,  $y = x^-/2$ . Corrections to this result are again  $\mathcal{O}(\alpha_s^3)$  in the exponent, and vanish when  $C_A = n_f = 0$ . Comparing Eq. (53) and (56) we explicitly observe the difference between the heavy quark jet function and the partonic shape function. Up to a sign the highest powers of  $\tilde{L}$  agree at each order in  $\alpha_s$ , because of the relation between their cusp anomalous dimension terms. The subleading logs and constant terms differ.

## V. A TRANSITIVE JET-MASS SCHEME

The last remaining ingredient needed for the NNLO and NNLL computations of the heavy-quark jet function is the specification of the mass scheme counterterm  $\delta m$  at two-loop order. Since the jet function will be used to describe momenta  $\hat{s} \sim \Gamma$ , where  $\Gamma$  is the width of the physical invariant mass distribution, we must have  $\delta m \sim \Gamma$  or smaller to not upset the power counting in the HQET Lagrangian, Eq. (7). In the  $\overline{\text{MS}}$  scheme  $\delta\overline{m} \sim m(\alpha_s + \alpha_s^2 + \dots)$ , and since  $m\alpha_s \gg \Gamma$  this scheme does not satisfy the power counting criteria. In the pole-mass scheme  $\delta m = 0$  to all orders, however this scheme has instabilities related to its infrared sensitivity. In particular the pole-mass has an infrared renormalon that leads to an asymptotic ambiguity  $\delta m^{\text{pole}} \sim \Lambda_{\text{QCD}}$ , and hence is not a useful scheme for precision computations. Schemes that satisfy  $\delta m \sim \Gamma$  and do not suffer from infrared renormalons were called top “jet-mass” schemes in Ref. [12]. We refer to them more generally as “top resonance mass-schemes” here and reserve the name jet-mass for a specific example of this type of scheme. These mass-schemes are suitable for use in the factorization theorem for the top-invariant mass distribution in Eq. (2) and related observables. We start by defining a jet-mass scheme with nice renormalization properties in section VA, and then relate this jet-mass to the pole,  $\overline{\text{MS}}$ , and 1S mass schemes in section VB.

### A. Potential Jet-Mass Definitions and Anomalous Dimensions

In this section we explore three resonance mass-schemes for  $m$ . With the notation for  $\delta m$  in Eq. (8) they are defined by

$$\begin{aligned}
 \text{a)} \quad & \frac{d}{d\hat{s}} B(\hat{s}, \delta m^{\text{peak}}, \Gamma_t, \mu) \Big|_{\hat{s}=0} = 0, \\
 \text{b)} \quad & \int_{-\infty}^R d\hat{s} \hat{s} B(\hat{s}, \delta m^{\text{mom}}, \mu) = 0, \\
 \text{c)} \quad & \delta m_J = \frac{-i}{2\tilde{B}(y, \mu)} \frac{d}{dy} \tilde{B}(y, \mu) \Big|_{y=-ie^{-\gamma_E}/R} = e^{\gamma_E} \frac{R}{2} \frac{d}{d\ln(iy)} \ln \tilde{B}(y, \mu) \Big|_{iy e^{\gamma_E}=1/R}.
 \end{aligned} \tag{57}$$

We refer to a), b), c) as the peak-mass, moment-mass, and position-mass respectively. The peak-mass definition uses the jet function with a non-zero width and satisfies the  $\delta m \sim \Gamma_t$  power counting criteria [12]. In b) and c) the schemes depend on a parameter  $R$ , and we must take  $R \sim \Gamma_t$  in order to satisfy the power counting criteria. Different choices for  $R$  specify different schemes, and are analogous to the difference between the  $\overline{\text{MS}}$  and  $\overline{\text{MS}}$  mass-schemes. All three schemes in Eq. (57) are free from leading renormalon ambiguities [65]. In the following we will argue that only the definition in c) is a reasonable scheme for higher order computations. Thus we will only use the name jet-mass for this position-scheme mass definition.

The definitions in Eq. (57) are all perturbative mass-schemes which stabilize the peak position of the jet function  $B(\hat{s}, \delta m, \Gamma_t, \mu)$ . In scheme a) the peak position is fixed to all orders in perturbation theory by definition. In scheme b) we instead fix the first moment, which provides a more local observable that is still sensitive to the peak location. However, scheme b) still has non-locality induced by the cutoff  $R$  on the momentum space moment. A finite  $R$  is necessary due to ultraviolet divergences that occur for  $R \rightarrow \infty$ . This type of moment divergence is a general property of functions that have a cusp anomalous dimension (see for example Refs. [66, 67]). If it was not for the UV divergences then the schemes b) and c) would be equivalent in the limit  $R \rightarrow \infty$ . In the situation at hand, c) provides an independent mass scheme definition. A jet-mass definition from c) is explicitly local since it just involves the position space jet function at a particular position  $y$ .

An additional criteria for a reasonable jet-mass scheme is to have a renormalization group evolution that is transitive, as discussed in Ref. [19]. Transitivity is a well-known feature of the  $\overline{\text{MS}}$  mass, and implies that we will obtain the same result if we evolve directly from  $\mu_0 \rightarrow \mu_2$ , or if we first evolve from  $\mu_0 \rightarrow \mu_1$  and then from  $\mu_1 \rightarrow \mu_2$ . Transitivity is guaranteed by any mass-scheme with a consistent anomalous dimension and renormalization group equation. Since in HQET the scale independent  $m^{\text{pole}} = m(\mu) + \delta m(\mu)$ , the general form for the RGE equation for the mass is

$$\mu \frac{d}{d\mu} m(\mu) = \gamma_m[R, m(\mu), \alpha_s(\mu)], \quad \gamma_m = -\mu \frac{d}{d\mu} \delta m(\mu), \tag{58}$$

where  $R$  is a mass dimension-1 scheme parameter. Transitivity of  $m(\mu)$  is guaranteed by this anomalous dimension equation, as long as  $\gamma_m$  is proportional to  $[m(\mu)]^k R^{1-k}$  for some  $k$  (and thus, for example, is not a sum of two types of terms with different powers of  $k$ ). In the  $\overline{\text{MS}}$  scheme  $k = 1$  and the anomalous dimension is proportional to  $m(\mu)$ , while in all three schemes in Eq. (57) we have  $k = 0$ . However, it turns out that the peak-scheme and moment-scheme do not have consistent anomalous dimension equations of the form in Eq. (58), because there  $\gamma_m$ 's depend on explicit powers  $\ln^j(\mu/\Gamma_t)$  and  $\ln^j(\mu/R)$  with higher and higher powers of  $j \geq 1$  occurring for higher orders in  $\alpha_s$ . These logs render the moment scheme anomalous dimension equation inconsistent at NLO order, and the peak scheme does not even have an anomalous dimension equation of the form in (58) at LO order.

In order to illustrate the difference between the three schemes in Eq. (57) we first consider the simplified case of the jet function in the abelian limit,  $C_A \rightarrow 0$  and  $n_f \rightarrow 0$ . The all-order result for  $\tilde{B}(y, \mu)$  is given in Eq. (54), and can be directly used to determine  $\delta m$  in the position-mass scheme. The derivative of the exponential gives back an exponential which cancels against the  $1/\tilde{B}(y, \mu)$  in  $\delta m_J$ . Thus the abelian result in the position-mass scheme is one-loop exact,

$$\delta m_J^{\text{abelian}} = e^{\gamma_E} R \frac{C_F \alpha_s}{\pi} \left[ \ln \frac{\mu}{R} + \frac{1}{2} \right]. \tag{59}$$

Since for the abelian limit  $d\alpha_s/d\mu = 0$ , the abelian anomalous dimension computed from Eq. (59) is  $(\gamma_m^J)^{\text{abelian}} = -R e^{\gamma_E} C_F \alpha_s / \pi$  to all orders. Thus this position-scheme anomalous dimension has the desired form in Eq. (58). To compute results for the peak and moment mass-schemes we need the abelian jet function in momentum space,  $B(\hat{s}, \mu)$ .

Tree, one-loop, and two-loop terms are given by the abelian terms in Eq. (39). To determine three-loop and higher order results we can simply expand Eq. (54) in  $\alpha_s$  and take the Fourier transform. For the three-loop term in the abelian jet function this gives

$$mB_3(\hat{s}, \mu)^{\text{abelian}} = C_F^3 \left[ \mathcal{L}^5 - \frac{5}{2} \mathcal{L}^4 + \left(4 - \frac{19\pi^2}{12}\right) \mathcal{L}^3 + \left(-\frac{7}{2} + \frac{19\pi^2}{8} + 20\zeta_3\right) \mathcal{L}^2 + \left(2 - \frac{15\pi^2}{8} + \frac{25\pi^4}{576} - 20\zeta_3\right) \mathcal{L}^1 \right. \\ \left. + \left(-\frac{1}{2} + \frac{13\pi^2}{24} - \frac{25\pi^4}{1152} + 8\zeta_3 - \frac{19\pi^2\zeta_3}{6} + 24\zeta_5\right) \mathcal{L}^0 + \left(\frac{1}{6} - \frac{7\pi^2}{48} + \frac{41\pi^4}{5760} - \frac{13777\pi^6}{2903040} - \frac{7\zeta_3}{3} + \frac{19\pi^2\zeta_3}{12} + \frac{20\zeta_3^2}{3} - 12\zeta_5\right) \delta(\hat{s}) \right]. \quad (60)$$

Using  $B_{0,1,2,3}(\hat{s}, \mu)^{\text{abelian}}$  we find that up to three-loop order

$$\delta m_{\text{abelian}}^{\text{peak}} = \frac{\pi\Gamma_t}{4} \left\{ \frac{C_F\alpha_s}{\pi} \left[ \ln \frac{\mu}{\Gamma_t} + \frac{3}{2} \right] + \frac{C_F^2\alpha_s^2}{\pi^2} \left[ -\ln^2 \frac{\mu}{\Gamma_t} + \left(\frac{\pi^2}{3} - 5\right) \ln \frac{\mu}{\Gamma_t} - \frac{13}{4} + \frac{\pi^2}{2} - 2\zeta_3 \right] + \frac{C_F^3\alpha_s^3}{\pi^3} \left[ \left(1 + \frac{\pi^2}{12}\right) \ln^3 \frac{\mu}{\Gamma_t} \right. \right. \\ \left. \left. + \left(\frac{25}{2} - \frac{5\pi^2}{12} - 4\zeta_3\right) \ln^2 \frac{\mu}{\Gamma_t} + \left(\frac{75}{4} - \frac{151\pi^2}{48} + \frac{11\pi^4}{45} - 8\zeta_3\right) \ln \frac{\mu}{\Gamma_t} + \frac{59}{8} - \frac{5\pi^2}{2} + \frac{11\pi^4}{30} + 5\zeta_3 - \pi^2\zeta_3 - 12\zeta_5 \right] \right\}, \\ \delta m_{\text{abelian}}^{\text{mom}} = R \left\{ \frac{C_F\alpha_s}{\pi} \left[ \ln \frac{\mu}{R} + \frac{3}{2} \right] + \frac{C_F^2\alpha_s^2}{\pi^2} \left[ \left(4 - \frac{\pi^2}{3}\right) \ln \frac{\mu}{R} + 8 - \frac{\pi^2}{2} - 2\zeta_3 \right] + \frac{C_F^3\alpha_s^3}{\pi^3} \left[ (6 - 4\zeta_3) \ln^2 \frac{\mu}{R} \right. \right. \\ \left. \left. + \left(46 - \frac{8\pi^2}{3} - \frac{\pi^4}{45} - 12\zeta_3\right) \ln \frac{\mu}{R} + \frac{159}{2} - \frac{16\pi^2}{3} - \frac{\pi^4}{30} - 21\zeta_3 + \frac{4\pi^2\zeta_3}{3} - 12\zeta_5 \right] \right\}. \quad (61)$$

At one-loop order the  $\delta m$  factors in the three schemes a), b), c) are quite similar.<sup>2</sup> However the three schemes are quite different at two-loop order. Computing  $\gamma_m$  from these counterterms we see that a  $\ln(\mu/\Gamma_t)$  appears in  $\gamma_m^{\text{peak}}$  at two-loop order, and that a  $\ln(\mu/R)$  appears in  $\gamma_m^{\text{mom}}$  at three-loop order. At higher orders in  $\alpha_s$ , higher and higher powers of these logarithms,  $\ln^j(\mu/R)$ , appear in  $\gamma_m$  in the peak and moment schemes. In particular we see from Eq. (61) that at three-loops for the peak-scheme there is a  $C_F^3 \ln^3(\mu/\Gamma_t)$  term that generates a  $\ln^2(\mu/\Gamma_t)$  in the computation of  $\gamma_m$ . For the moment scheme we have extended the abelian computation to four-loops, and find a term

$$(\delta m_{\text{abelian}}^{\text{mom}})^{4\text{loop}} = R \frac{C_F^4\alpha_s^4}{\pi^4} \left[ \left(\frac{32}{3} - \frac{4\pi^4}{45}\right) \ln^3 \frac{\mu}{R} + \dots \right]. \quad (62)$$

This gives a  $\ln^2(\mu/R)$  in the moment scheme  $\gamma_m$  at four-loop order.<sup>3</sup> The absence of  $\alpha_s^k \ln^k(\mu/R)$  terms in  $\delta m_{\text{abelian}}^{\text{mom}}$  is a reflection of the fact that the moment-mass has a consistent anomalous dimension at LO. Neither the peak-scheme nor the moment-scheme have consistent anomalous dimension equations in general. This inconsistency arises because of the non-locality inherent in their definitions. This is problematic because we would like to be able to evolve our mass as a function of  $\mu$ , for instance to run it up to large mass scales and connect it to the  $\overline{\text{MS}}$  scheme at a scale  $\mu = m_t$ . On the other hand the position-scheme is entirely local, and so far we have demonstrated that in the abelian limit it has a consistent mass anomalous dimension. We extend this proof to the non-abelian case below.

In table I we present non-abelian results for the two-loop computation of  $\delta m$  for all three schemes in Eq. (57). The position-scheme jet-mass is no longer one-loop exact, and has corrections at each order in  $\alpha_s(\mu)$ . Since now the coupling  $\alpha_s(\mu)$  evolves, higher powers of  $\ln^j(\mu/R)$  are unavoidable. In order for the scheme to yield an anomalous dimension of the form in Eq. (58) these higher powers must appear along with  $\beta_i$  coefficients in just the right way to ensure that the  $\ln(\mu/R)$  terms do not appear in  $\gamma_m$ . This is precisely what happens for the position-scheme (jet-mass scheme) at two-loop order. Note that the main difference between the moment scheme and the jet-mass scheme is the presence of  $C_F^2$  terms in  $\delta m^{\text{mom}}$ , but that there are also differences in the subleading log and constant  $C_F\beta_0$  terms at two-loops. In Ref. [19] it was proven by an explicit construction at LL order that the moment-mass has a consistent anomalous dimension which sums the leading logs. Thus the one-loop analysis in Ref. [19] (which used the moment-mass) is fully consistent. However, beyond one-loop order it is mandatory to use the position-scheme definition of the jet-mass given in Eq. (57)c.

<sup>2</sup> In the position-scheme it might appear that there is a freedom in the overall normalization of  $\delta m$  in Eq. (57)c, and in the choice of  $R$ . In fact to obtain a renormalon free jet-mass scheme there is no freedom in the overall normalization, there is only freedom in the choice of  $R$  [65].

<sup>3</sup> The presence of these higher logs in  $\gamma_m$  for the peak and moment schemes implies that these masses also do not fall into the cusp-anomalous dimension category, which requires an anomalous dimension of the form  $\gamma_m = R\gamma_1[\alpha_s] + R\ln(\mu/R)\gamma_2[\alpha_s]$ , i.e. with just a single  $\ln(\mu/R)$  to all orders in  $\alpha_s$ .

order	peak scheme $\frac{4}{\pi\Gamma_t} \delta m^{\text{peak}} =$	moment scheme $\frac{1}{R} \delta m^{\text{mom}} =$	jet-mass scheme $e^{-\gamma_E} \frac{1}{R} \delta m_J =$
$\alpha_s/\pi$	$C_F \left[ \ln \frac{\mu}{\Gamma_t} + \frac{3}{2} \right]$	$C_F \left[ \ln \frac{\mu}{R} + \frac{3}{2} \right]$	$C_F \left[ \ln \frac{\mu}{R} + \frac{1}{2} \right]$
$\alpha_s^2/\pi^2$	$C_F^2 \left[ -\ln^2 \frac{\mu}{\Gamma_t} + \left( \frac{\pi^2}{3} - 5 \right) \ln \frac{\mu}{\Gamma_t} - \frac{13}{4} + \frac{\pi^2}{2} - 2\zeta_3 \right]$ $+ C_F \beta_0 \left[ \frac{1}{4} \ln^2 \frac{\mu}{\Gamma_t} + \frac{7}{6} \ln \frac{\mu}{\Gamma_t} + \frac{95}{72} + \frac{\pi^2}{48} \right]$ $+ C_F C_A \left[ \left( \frac{1}{3} - \frac{\pi^2}{12} \right) \ln \frac{\mu}{\Gamma_t} + \frac{17}{36} - \frac{\pi^2}{8} - \frac{5}{8} \zeta_3 \right]$	$C_F^2 \left[ \left( 4 - \frac{\pi^2}{3} \right) \ln \frac{\mu}{R} + 8 - \frac{\pi^2}{2} - 2\zeta_3 \right]$ $+ C_F \beta_0 \left[ \frac{1}{4} \ln^2 \frac{\mu}{R} + \frac{7}{6} \ln \frac{\mu}{R} + \frac{131}{72} - \frac{\pi^2}{24} \right]$ $+ C_F C_A \left[ \left( \frac{1}{3} - \frac{\pi^2}{12} \right) \ln \frac{\mu}{R} + \frac{17}{36} - \frac{\pi^2}{8} - \frac{5}{8} \zeta_3 \right]$	0 $+ C_F \beta_0 \left[ \frac{1}{4} \ln^2 \frac{\mu}{R} + \frac{2}{3} \ln \frac{\mu}{R} + \frac{47}{72} \right]$ $+ C_F C_A \left[ \left( \frac{1}{3} - \frac{\pi^2}{12} \right) \ln \frac{\mu}{R} + \frac{5}{36} - \frac{\pi^2}{24} - \frac{5}{8} \zeta_3 \right]$

TABLE I: Coefficients of the HQET counterterm  $\delta m$  for different mass schemes at one and two-loop order.

Lets extend the proof of consistency of the anomalous dimension in the position-scheme (jet-mass scheme) to the full non-abelian case. At the same time we will derive the very nice result that  $\gamma_m$  for the jet-mass scheme is entirely determined by the cusp-anomalous dimension. To all orders in perturbation theory, using Eq. (57), the jet-mass anomalous dimension is

$$\gamma_m^J = -\frac{d\delta m(\mu)}{d\ln\mu} = -e^{\gamma_E} \frac{R}{2} \frac{d}{d\ln\mu} \frac{d}{d\ln(iy)} \ln \tilde{B}(y, \mu) \Big|_{iy e^{\gamma_E} = 1/R}. \quad (63)$$

Using Eq. (55) and then Eq. (26) this gives  $[\mu_y = e^{-\gamma_E}/(iy)]$

$$\begin{aligned} \gamma_m^J &= -e^{\gamma_E} \frac{R}{2} \frac{d}{d\ln\mu} \frac{d}{d\ln(iy)} K(\mu, \mu_y) = e^{\gamma_E} \frac{R}{2} \frac{d}{d\ln\mu} \frac{d}{d\ln\mu_y} K(\mu, \mu_y) \\ &= e^{\gamma_E} R \beta[\alpha_s(\mu)] \beta[\alpha_s(\mu_y)] \frac{d^2}{d\alpha_s(\mu_y) d\alpha_s(\mu)} \int_{\alpha_s(\mu_y)}^{\alpha_s(\mu)} \frac{d\alpha}{\beta[\alpha]} \Gamma^c[\alpha] \int_{\alpha_s(\mu_y)}^{\alpha} \frac{d\alpha'}{\beta[\alpha']}, \end{aligned} \quad (64)$$

where we should evaluate the final result at  $\mu_y = R$ . Performing the derivatives with respect to the couplings we see that at any order in perturbation theory the anomalous dimension for  $m_J(\mu)$  is actually independent of  $\mu_y$ . Furthermore the result is given by the cusp-anomalous dimension,  $\gamma_m = -e^{\gamma_E} R \Gamma^c[\alpha_s(\mu)]$ . Thus, to all orders in perturbation theory the jet-mass scheme, defined by c) in Eq. (57), has a consistent anomalous dimension as in Eq. (58), and yields a transitive running mass,  $m_J(\mu)$ . The final anomalous dimension equation for the jet-mass is

$$\frac{dm_J(\mu)}{d\ln\mu} = -e^{\gamma_E} R \Gamma^c[\alpha_s(\mu)], \quad (65)$$

and is fully determined by the cusp-anomalous dimension. The all-orders solution of this equation is

$$m_J(\mu) = m_J(\mu_0) - \frac{e^{\gamma_E} R}{2} \omega(\mu, \mu_0). \quad (66)$$

Since  $\Gamma^c$  is known to three-loop order we can use Eq. (42) to obtain the running jet-mass at NNLL

$$\begin{aligned} m_J(\mu) &= m_J(\mu_0) + e^{\gamma_E} R \frac{2C_F}{\beta_0} \ln \left[ \frac{\alpha_s(\mu)}{\alpha_s(\mu_0)} \right] + e^{\gamma_E} R \left( \frac{\Gamma_1^c}{\beta_0} - \frac{\beta_1 \Gamma_0^c}{\beta_0^2} \right) \left[ \frac{\alpha_s(\mu) - \alpha_s(\mu_0)}{8\pi} \right] \\ &+ e^{\gamma_E} R \left( \frac{\Gamma_2^c}{\beta_0} - \frac{\Gamma_1^c \beta_1}{\beta_0^2} + \frac{\Gamma_0^c \beta_1^2}{\beta_0^3} - \frac{\Gamma_0^c \beta_2}{\beta_0^2} \right) \left[ \frac{\alpha_s^2(\mu) - \alpha_s^2(\mu_0)}{64\pi^2} \right]. \end{aligned} \quad (67)$$

Note that the form of the anomalous dimension in  $\mu d/d\mu [m_J(\mu)/R]$  has the same structure as that in  $\mu d/d\mu [\ln \overline{m}(\mu)]$ , where  $\overline{m}(\mu)$  is the  $\overline{\text{MS}}$  mass. In the remaining sections we will use the position mass-scheme and refer to it exclusively as the jet-mass.

## B. Relating the Jet-Mass to other Mass Schemes

Having obtained a suitable mass definition for measurements of the top-mass from jets, we now turn to perturbatively connecting it to other schemes. Using the result for  $\delta m_J$  from Table I we obtain the two-loop relation between the

jet-mass and pole-mass

$$m_{\text{pole}} = m_J(\mu) + e^{\gamma_E} R \frac{\alpha_s(\mu) C_F}{\pi} \left[ \ln \frac{\mu}{R} + \frac{1}{2} \right] + e^{\gamma_E} R \frac{\alpha_s^2(\mu)}{\pi^2} \left\{ C_F \beta_0 \left[ \frac{1}{4} \ln^2 \frac{\mu}{R} + \frac{2}{3} \ln \frac{\mu}{R} + \frac{47}{72} \right] + C_F C_A \left[ \left( \frac{1}{3} - \frac{\pi^2}{12} \right) \ln \frac{\mu}{R} + \frac{5}{36} - \frac{\pi^2}{24} - \frac{5}{8} \zeta_3 \right] \right\}. \quad (68)$$

This relation can be compared to other well known two-loop mass relations, such as i) between the pole-mass and  $\overline{\text{MS}}$ -mass [68, 69],

$$m_{\text{pole}} = \overline{m}(\mu) \left\{ 1 + \frac{C_F \alpha_s(\mu)}{\pi} \left[ 1 + \frac{3}{2} \ln \frac{\mu}{\overline{m}} \right] + \frac{\alpha_s^2(\mu)}{\pi^2} \left[ C_F \beta_0^{(n_f+1)} \left( \frac{3}{8} \ln^2 \frac{\mu}{\overline{m}} + \frac{13}{16} \ln \frac{\mu}{\overline{m}} + \frac{71}{128} + \frac{\pi^2}{16} \right) + C_F \left( \frac{\pi^2 - 3}{8} \right) + C_F C_A \left( \frac{7}{8} \ln \frac{\mu}{\overline{m}} + \frac{55}{64} - \frac{5\pi^2}{16} + \frac{\pi^2 \ln 2}{4} - \frac{3\zeta_3}{8} \right) + C_F^2 \left( \frac{9}{8} \ln^2 \frac{\mu}{\overline{m}} - \frac{9}{16} \ln \frac{\mu}{\overline{m}} - \frac{71}{128} + \frac{5\pi^2}{16} - \frac{\pi^2 \ln 2}{2} + \frac{3\zeta_3}{4} \right) \right] \right\}, \quad (69)$$

where  $\overline{m} = \overline{m}(\mu)$ ,  $\beta_0^{(n_f+1)} = \beta_0 - 2/3$ , and  $\alpha_s(\mu)$  here is in the  $(n_f + 1)$ -flavor theory, and ii) between the pole-mass and 1S-mass [6],

$$m_{\text{pole}} = m^{1S} \left\{ 1 + \frac{C_F^2 \alpha_s^2(\mu)}{8} + \frac{C_F^2 \alpha_s^3(\mu)}{8\pi} \left[ \beta_0 \ln \left( \frac{\mu}{C_F \alpha_s(\mu) m^{1S}} \right) + \frac{11\beta_0}{6} - \frac{4C_A}{3} \right] \right\}. \quad (70)$$

Here  $\alpha_s(\mu)$  is in the  $n_f$ -flavor theory. Note that in Eqs. (69) and (70) we have  $n_f = 5$  light massless flavors, and thus did not write for example vacuum polarization terms depending on the b-quark mass.

Lets imagine that the jet-mass  $m_J(\mu_J)$  is determined from a fit to massive event shapes using a scale  $\mu_J \sim \Gamma$ . In order to connect this  $m_J(\mu_J)$  to the high-energy  $\overline{\text{MS}}$ -mass, we proceed as follows. First because the renormalization group evolution of the  $\overline{\text{MS}}$ -mass does not make sense below the mass itself, we evolve the jet-mass  $m_J(\mu_J)$  up to the scale  $\overline{m}_t = \overline{m}(\overline{m}_t)$  to obtain  $m_J(\overline{m}_t)$  using the NNLL running result in Eq. (67). At this scale we then connect the jet and  $\overline{\text{MS}}$ -masses by eliminating the pole mass from Eqs. (68,69). Thus the two-loop relation between the jet-mass and  $\overline{\text{MS}}$ -mass is

$$\overline{m}(\overline{m}_t) = m_J(\overline{m}_t) + \left\{ e^{\gamma_E} R \frac{\alpha_s(\overline{m}_t) C_F}{\pi} \left[ \ln \frac{\overline{m}_t}{R} + \frac{1}{2} \right] - m_J(\overline{m}_t) \frac{\alpha_s(\overline{m}_t) C_F}{\pi} \right\} + \left\{ -m_J(\overline{m}_t) \frac{\alpha_s^2(\overline{m}_t)}{\pi^2} \left[ C_F \left( \frac{\pi^2}{12} - \frac{143}{192} \right) + C_F \beta_0 \left( \frac{71}{128} + \frac{\pi^2}{16} \right) + C_F C_A \left( \frac{55}{64} - \frac{5\pi^2}{16} + \frac{\pi^2 \ln 2}{4} - \frac{3\zeta_3}{8} \right) + C_F^2 \left( \frac{5\pi^2}{16} - \frac{199}{128} - \frac{\pi^2 \ln 2}{2} + \frac{3\zeta_3}{4} \right) \right] + e^{\gamma_E} R \frac{\alpha_s^2(\overline{m}_t)}{\pi^2} \left[ C_F \beta_0 \left[ \frac{1}{4} \ln^2 \frac{\overline{m}_t}{R} + \frac{2}{3} \ln \frac{\overline{m}_t}{R} + \frac{47}{72} \right] + C_F C_A \left[ \left( \frac{1}{3} - \frac{\pi^2}{12} \right) \ln \frac{\overline{m}_t}{R} + \frac{5}{36} - \frac{\pi^2}{24} - \frac{5}{8} \zeta_3 \right] - C_F^2 \left[ \ln \frac{\overline{m}_t}{R} + \frac{1}{2} \right] \right] \right\}. \quad (71)$$

Since we take  $\mu = \overline{m}_t$  there is no threshold correction at the order we are working, and  $\alpha_s(\overline{m}_t)$  in Eq. (71) is the same in the  $n_f$  and  $(n_f + 1)$ -flavor theories. Together with Eq. (67) this formula inputs a jet-mass determined from production of tops far above threshold, and outputs an  $\overline{\text{MS}}$  mass that can be used in other processes, such as the analysis of precision electroweak data. Since a high precision result for the top-mass in the 1S mass-scheme can be determined from a threshold cross-section analysis, we also quote the two-loop conversion between the jet-mass and 1S-mass schemes. An extra power of  $\alpha_s$  is kept in the 1S-scheme terms to properly ensure a renormalon free series [6]. At a scale  $\mu$  the conversion at second order is

$$m_t^{1S} = m_J(\mu) + \left\{ e^{\gamma_E} R \frac{\alpha_s(\mu) C_F}{\pi} \left[ \ln \frac{\mu}{R} + \frac{1}{2} \right] - m_J(\mu) \frac{\alpha_s^2(\mu) C_F^2}{8} \right\} + \left\{ -e^{\gamma_E} R \frac{\alpha_s^3(\mu) C_F^3}{8\pi} \left[ \ln \frac{\mu}{R} + \frac{1}{2} \right] - m_J(\mu) \frac{\alpha_s^3(\mu) C_F^2}{8\pi} \left[ \beta_0 \ln \left( \frac{\mu}{C_F \alpha_s(\mu) m_J(\mu)} \right) + \frac{11\beta_0}{6} - \frac{4C_A}{3} \right] + e^{\gamma_E} R \frac{\alpha_s^2(\mu)}{\pi^2} \left[ C_F \beta_0 \left[ \frac{1}{4} \ln^2 \frac{\mu}{R} + \frac{2}{3} \ln \frac{\mu}{R} + \frac{47}{72} \right] + C_F C_A \left[ \left( \frac{1}{3} - \frac{\pi^2}{12} \right) \ln \frac{\mu}{R} + \frac{5}{36} - \frac{\pi^2}{24} - \frac{5}{8} \zeta_3 \right] \right] \right\}. \quad (72)$$

## VI. RESULTS FOR THE NNLL JET FUNCTION

In this section we present the final result for the heavy quark jet function  $B(\hat{s}, \delta m, \Gamma_t, \mu)$ , with NNLO perturbative corrections and a NNLL resummation of large logs. We study the numerical effect of these two-loop corrections as



well as of the log-resummation, including the perturbative convergence and  $\mu$ -dependence of  $B$  as a function of  $\hat{s}$ , and in particular the stability of its peak position which is important for a top-mass measurement. At tree-level  $B(\hat{s}, \delta m, \mu) = \delta(\hat{s})$  and we see from Eq. (12) that  $B(\hat{s}, \delta m, \Gamma_t, \mu)$  is simply a Breit-Wigner centered at  $\hat{s} = 0$  with a width  $\Gamma_t$ . Beyond tree-level the jet function becomes dependent on  $\mu$  and on the choice of mass-scheme through  $\delta m$ .

For the cross-section  $d^2\sigma/dM_t^2 dM_{\bar{t}}^2$  in Eq. (2) it has been proven that at any order in perturbation theory, the only large logs that effect the shape of the invariant mass distribution are those due to the resummation in the heavy-quark jet function [19].<sup>4</sup> Furthermore these large logs only exist between scales  $\mu_\Gamma \sim \Gamma \equiv \Gamma_t + Q\Lambda_{\text{QCD}}/m$  and  $\mu_\Lambda \gtrsim \Lambda_{\text{QCD}} + m\Gamma_t/Q$ . The remaining large logs only modify the cross-sections normalization. The expression which resums all logs between the scales  $\mu_Q \simeq Q \gg \mu_m \simeq m \gg \mu_\Gamma \simeq \Gamma \gg \mu_\Lambda \gtrsim \Lambda_{\text{QCD}}$  is

$$\begin{aligned} \frac{d^2\sigma}{dM_t dM_{\bar{t}}} &= 4\sigma_0 M_t M_{\bar{t}} H_Q(Q, \mu_Q) U_{H_Q}(Q, \mu_Q, \mu_m) H_m(m_J, \mu_m) U_{H_m}(Q/m_J, \mu_m, \mu_\Lambda) \\ &\times \int_{-\infty}^{+\infty} d\ell^+ d\ell^- B_+ \left( \hat{s}_t - \frac{Q\ell^+}{m_J}, \delta m_J, \Gamma_t, \mu_\Lambda, \mu_\Gamma \right) B_- \left( \hat{s}_{\bar{t}} - \frac{Q\ell^-}{m_J}, \delta m_J, \Gamma_t, \mu_\Lambda, \mu_\Gamma \right) S(\ell^+, \ell^-, \mu_\Lambda, \delta, \bar{\Delta}(\mu_\Lambda)), \end{aligned} \quad (73)$$

where we have defined the resummed jet function as

$$\begin{aligned} B(\hat{s}, \delta m_J, \Gamma_t, \mu_\Lambda, \mu_\Gamma) &\equiv \int d\hat{s}' U_B(\hat{s} - \hat{s}', \mu_\Lambda, \mu_\Gamma) B(\hat{s}', \delta m_J, \Gamma_t, \mu_\Gamma) \\ &= \int d\hat{s}' d\hat{s}'' U_B(\hat{s} - \hat{s}', \mu_\Lambda, \mu_\Gamma) B(\hat{s}' - \hat{s}'', \delta m_J, \mu_\Gamma) \frac{\Gamma_t}{\pi(\hat{s}''^2 + \Gamma_t^2)}. \end{aligned} \quad (74)$$

In Eqs. (73,74) large logs are resummed by the evolution factors  $U_{H_Q}$ ,  $U_{H_m}$ , and  $U_B$ , and of these, the first two only affect the overall normalization. Since the scales  $\mu_\Gamma$  and  $\mu_\Lambda$  differ by a factor of  $Q/m$  it is necessary to sum the large logs between these scales. Recall that Eq. (73) is valid for  $Q \gg m$ , which is mandatory for the top quark and antitop quarks to decay to well separated jets. The numerical importance of this particular resummation has already been demonstrated at NLL order in Ref. [19].

In the following we study the resummed jet function  $B(\hat{s}, \delta m, \Gamma_t, \mu_\Lambda, \mu_\Gamma)$  and its dependence on  $\hat{s}$  and  $\mu_\Gamma$ . In particular the  $\mu_\Gamma$  dependence cancels out order-by-order in renormalization group improved perturbation theory, and thus the residual  $\mu_\Gamma$  dependence provides a method for estimating the effect of higher order corrections to the jet function. This  $\mu_\Gamma$  dependence cancels order-by-order between the evolver  $U_B(\hat{s} - \hat{s}', \mu_\Lambda, \mu_\Gamma)$  and the fixed-order jet function matrix element that gives  $B(\hat{s}' - \hat{s}'', \delta m, \mu_\Gamma)$  in Eq. (74). On the other hand, the dependence of the resummed jet function on  $\mu_\Lambda$  cancels out only in the complete cross-section, where there is additional dependence on  $\mu_\Lambda$  in both the evolution function  $U_{H_m}$  and the soft-function  $S$ . The analysis of the invariant mass dependence of the full NNLL cross-section requires constructing a consistent model for the soft-function at two-loop order, since  $S$  contains both perturbative and non-perturbative pieces. The procedure in Ref. [22] can be used to carry out this analysis, but we leave the study of the full cross-section to a future publication. Here we focus on the resummed jet function.

Following the strategy in appendix E of Ref. [19] we can obtain analytic results for the NNLL jet function even in the presence of the width. At NNLL order we find

$$\begin{aligned} mB(\hat{s}, \delta m, \Gamma_t, \mu_\Lambda, \mu_\Gamma) &= G_0 + \frac{C_F \alpha_s(\mu_\Gamma)}{\pi} \left[ G_2 - G_1 + \left( 1 + \frac{5\pi^2}{24} \right) G_0 \right] - \frac{2\alpha_s(\mu_\Gamma)}{\pi} \delta m_1(\mu_\Gamma) (G_0)' \\ &+ \frac{\alpha_s^2(\mu_\Gamma)}{\pi^2} \left\{ C_F^2 \left[ \frac{1}{2} G_4 - G_3 + \left( \frac{3}{2} + \frac{13\pi^2}{24} \right) G_2 - \left( 1 + \frac{13\pi^2}{24} - 4\zeta_3 \right) G_1 + \left( \frac{1}{2} + \frac{7\pi^2}{24} + \frac{53\pi^4}{640} - 2\zeta_3 \right) G_0 \right] \right. \\ &\quad + C_F C_A \left[ \left( \frac{1}{3} - \frac{\pi^2}{12} \right) G_2 - \left( \frac{5}{18} - \frac{\pi^2}{12} - \frac{5\zeta_3}{4} \right) G_1 + \left( -\frac{11}{54} + \frac{5\pi^2}{48} - \frac{19\pi^4}{960} - \frac{5\zeta_3}{8} \right) G_0 \right] \\ &\quad \left. + C_F \beta_0 \left[ -\frac{1}{6} G_3 + \frac{2}{3} G_2 - \left( \frac{47}{36} + \frac{\pi^2}{12} \right) G_1 + \left( \frac{281}{216} + \frac{23\pi^2}{192} - \frac{17\zeta_3}{48} \right) G_0 \right] \right\} \\ &- \frac{2\alpha_s^2(\mu_\Gamma)}{\pi^2} \left\{ \delta m_2 (G_0)' - (\delta m_1)^2 (G_0)'' + \delta m_1 C_F \left[ (G_2)' - (G_1)' + \left( 1 + \frac{5\pi^2}{24} \right) (G_0)' \right] \right\}. \end{aligned} \quad (75)$$

<sup>4</sup> In principle both the logs in the jet function and in the soft-function can modify the invariant mass distribution. However due to the consistency conditions discussed in Ref. [19] it is always possible to exchange a summation of large logs in the soft function in favor of large logs in the jet function and in the hard function normalization factors.

The result is expressed in terms of the functions  $G_n = G_n(\hat{s}, \Gamma_t, \mu_\Lambda, \mu_\Gamma)$  and their  $\hat{s}$  derivatives, with

$$G_n = \frac{1}{\pi} \text{Im} \left[ \frac{e^{K(\mu_\Gamma e^{\gamma_E})^\omega} \Gamma(1+\omega)}{(-\hat{s} - i\Gamma_t)^{1+\omega}} I_n \left( \frac{\hat{s} + i\Gamma_t}{\mu_\Gamma}, \omega \right) \right]. \quad (76)$$

Here  $\omega = \omega(\mu_\Lambda, \mu_\Gamma)$  and  $K = K(\mu_\Lambda, \mu_\Gamma)$  are given in Eq. (42) and

$$\begin{aligned} I_0(x, \omega) &= 1, \\ I_1(x, \omega) &= \ln(-x-i0) - H(\omega), \\ I_2(x, \omega) &= [\ln(-x-i0) - H(\omega)]^2 + \psi^{(1)}(1+\omega) - \zeta_2, \\ I_3(x, \omega) &= [\ln(-x-i0) - H(\omega)]^3 + 3[\psi^{(1)}(1+\omega) - \zeta_2][\ln(-x-i0) - H(\omega)] + \psi^{(2)}(1) - \psi^{(2)}(1+\omega), \\ I_4(x, \omega) &= [\ln(-x-i0) - H(\omega)]^4 + 6[\psi^{(1)}(1+\omega) - \zeta_2][\ln(-x-i0) - H(\omega)]^2 \\ &\quad - 4[\psi^{(2)}(1+\omega) - \psi^{(2)}(1)][\ln(-x-i0) - H(\omega)] + \psi^{(3)}(1+\omega) - \psi^{(3)}(1) + 3[\psi^{(1)}(1+\omega) - \zeta_2]^2, \end{aligned} \quad (77)$$

with  $H(\omega)$  the harmonic-number function, and  $\psi^{(k)}(x)$  the  $k$ 'th derivative of the digamma function or equivalently the  $(k+1)$ 'th derivative of the log of the gamma function.

We focus our numerical analysis on two mass schemes for the jet function. In the pole scheme we take  $\delta m_1 = \delta m_2 = 0$  in Eq. (75) and use a fixed pole mass  $m = m^{\text{pole}} = 172 \text{ GeV}$  in the formula for  $\hat{s}$  in Eq. (3). In the jet-mass scheme we use  $\delta m_1$  and  $\delta m_2$  from the last column of Table I with a scheme parameter  $R = 0.8 \text{ GeV}$  that corresponds to a scale  $e^{\gamma_E} R \simeq 1.4 \text{ GeV}$ . Here  $m = m_J(\mu_\Gamma)$  is the mass in the jet-scheme, and

$$\hat{s} = \frac{M_t^2 - m_J^2(\mu_\Gamma)}{m_J(\mu_\Gamma)}. \quad (78)$$

The value of  $m_J(\mu_\Gamma)$  to be used here is obtained using the evolution equation in Eq. (67), running up from an input scale  $\mu_0$ . For this scheme it is the parameter  $m_J(\mu_0)$  that one will extract with future linear-collider data. In our analysis we take  $\mu_0 = 2 \text{ GeV}$  and simply fix  $m_J(\mu_0) = 172 \text{ GeV}$ . We use the three-loop result for the running coupling everywhere,

$$\frac{1}{\alpha_s(\mu)} = \frac{X}{\alpha_s(\mu_0)} + \frac{\beta_1}{4\pi\beta_0} \ln X + \frac{\alpha_s(\mu_0)}{16\pi^2} \left[ \frac{\beta_1^2}{\beta_0^2} \left( \frac{\ln X}{X} + \frac{1}{X} - 1 \right) + \frac{\beta_2}{\beta_0} \left( 1 - \frac{1}{X} \right) \right], \quad (79)$$

where  $X \equiv 1 + \alpha_s(\mu_0)\beta_0 \ln(\mu/\mu_0)/(2\pi)$  and we evolve to lower scales using the reference value  $\alpha_s(\mu_0 = m_Z) = 0.118$  with  $n_f = 5$ . Since we have systematically treated the  $b$ -quark as massless we also ignore the  $b$ -quark threshold in our coupling evolution. We also fix  $\Gamma_t = 1.43 \text{ GeV}$ , and  $\mu_\Lambda = 1 \text{ GeV}$ . For  $\mu_\Gamma$  we take a central value of  $\mu_\Gamma = 5 \text{ GeV}$  and consider variations about this scale in the range  $3.3 \text{ GeV} < \mu_\Gamma < 7.5 \text{ GeV}$ . Even though it may slightly underestimate higher-order uncertainties, we have chosen not to make the canonical choice of varying  $\mu_\Gamma$  up and down by a factor of two because of the importance of retaining the hierarchy  $\mu_\Gamma/\mu_\Lambda \simeq Q/m_J$  as emphasized in Ref. [19].

In Fig. 3 we plot the resummed heavy-quark jet function  $B(\hat{s}, \delta m, \Gamma_t, \mu_\Lambda, \mu_\Gamma)$  versus  $M_t$ . In the left panel we show results for the pole scheme, and in the right panel we show results for the jet-scheme. In each panel we plot tree level results (black dotted-line), LL results (green short-dashed lines), NLL results (blue long-dashed lines), and NNLL results (solid red lines). The tree results are the pure Breit-Wigner, the LL results use the tree-level  $B(\hat{s}, \delta m, \mu)$  with the LL result for  $U_B$  in Eq. (74), and thus correspond to just the first  $G_0$  term in Eq. (75). From the LL results we see that beyond tree-level the jet function grows a perturbative tail above the peak. The NLL results use the one-loop  $B$  with the NLL result for  $U_B$  and thus include the  $\mathcal{O}(\alpha_s(\mu_\Gamma))$  terms in Eq. (75), and the NNLL curves use the two-loop  $B$  with the NNLL result for  $U_B$  and thus all of the terms in Eq. (75). At each of the LL, NLL, and NNLL orders we show three curves with  $\mu_\Gamma = 3.3, 5.0, 7.5 \text{ GeV}$ , which are the curves from top to bottom near the peak respectively. Recall that in the jet scheme we fix  $m_J(\mu_0 = 2 \text{ GeV}) = 172 \text{ GeV}$  and use the solution of the mass renormalization group equation in Eq. (67). Thus the conversion from  $M_t$  to  $\hat{s}$  depends on the value of  $\mu_\Gamma$  and order-by-order compensates for the  $\mu_\Gamma$  dependence of the residual mass terms  $\delta m_{1,2}(\mu_\Gamma)$ .

Examining the LL, NLL, and NNLL results for the jet function in Fig. 3 we observe that the jet-scheme results in the second panel exhibit better perturbative convergence than the pole-scheme results in the first panel. This is true of all features, including the slope to the left of the peak, the perturbative tail to right of the peak, the peak location, and the peak height. Comparing the spread of the curves we see that at both NLL and NNLL order the

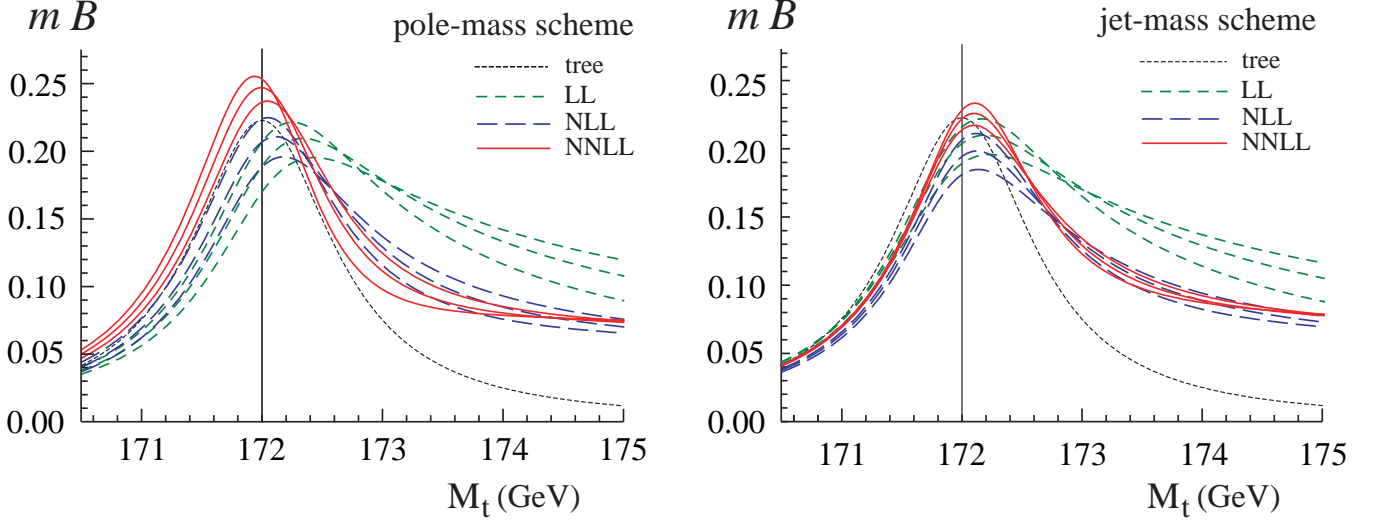


FIG. 3: The jet function,  $mB(\hat{s}, \delta m, \Gamma_t, \mu)$  versus  $M_t$ , where  $\hat{s} = (M_t^2 - m^2)/m$  and  $\Gamma_t = 1.43$  GeV. The left panel shows results in the pole-mass scheme and the right panel shows results in the jet-mass scheme. The black dotted curve is the tree-level Breit-Wigner, the green short-dashed curves are LL results, blue long-dashed curves are NLL, and the solid red curves are at NNLL order. For each of the LL, NLL, and NNLL results we show three curves with  $\mu_\Gamma = 3.3, 5.0, 7.5$  GeV respectively. Other parameters are discussed in the text.

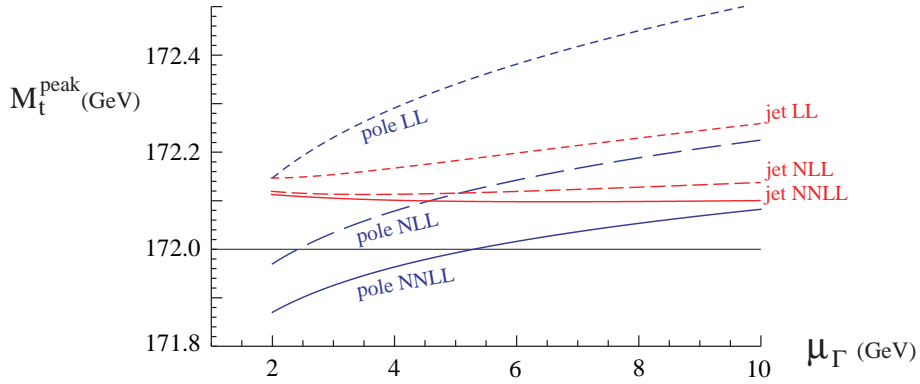


FIG. 4: Peak position  $M_t^{\text{peak}}$  of the jet function versus  $\mu_\Gamma$ . Short-dashed results are at LL order, long-dashed are at NLL order, and solid are at NNLL order. Results are labeled for the pole mass-scheme (blue) and jet mass-scheme (red).

residual  $\mu_\Gamma$  dependence is smaller in the jet-scheme than in the pole-scheme. The numerical size of the residual  $\mu_\Gamma$  scale dependence varies region by region. In the pole-mass scheme the scale dependence in the slope before the peak is  $\sim 17\%$  at NLL and  $\sim 14\%$  at NNLL, while the maximum variation near the peak is  $23\%$  at NLL and  $17\%$  at NNLL, and then in the tail region well above the peak it is  $\sim 19\%$  at NLL and  $\sim 13\%$  at NNLL. Hence, in the pole scheme including the NNLL results does not significantly decrease the  $\mu_\Gamma$  dependence. In the jet-mass scheme the scale dependence in the slope before the peak is  $\sim 6\%$  at NLL and  $\sim 2\%$  at NNLL, while the maximum variation near the peak is  $14\%$  at NLL and  $7\%$  at NNLL, and then in the tail above the peak it is  $\sim 12\%$  at NLL and  $\sim 5\%$  at NNLL. Thus, in the jet-mass scheme the  $\mu_\Gamma$  dependence is reduced by a factor of two or more. The same level of improvement is observed for different values of the scheme parameter  $R$  than the value used in our analysis.

In Fig. 4 we plot the peak position  $M_t^{\text{peak}}$  of the jet function curves, versus  $\mu_\Gamma$ . This figure displays the convergence and  $\mu_\Gamma$  dependence of the jet function peak position in more detail than Fig. 3. The stability of the jet function peak has a direct influence on the peak of the cross-section, and both are very sensitive to the value of the short-distance top-mass. Hence the peak-position is important to gauge the effect of perturbative corrections for the mass measurement. We use a wider range for  $\mu_\Gamma$  than that of the curves in Fig. 3, but note that results for  $\mu_\Gamma \leq 3$  GeV upset the hierarchy  $\mu_\Gamma/\mu_\Lambda \simeq 5$  and hence can be safely ignored. In the pole-mass scheme we observe that there is limited sign of convergence for the peak position, although the shifts with  $\mu_\Gamma = 5$  GeV at each order are still relatively small being  $\simeq 230$  MeV from LL to NLL order and  $\simeq 120$  MeV from NLL to NNLL order. The lack of convergence

of the peak-position in the pole-scheme is a reflection of the infrared renormalon in the pole-mass, which destabilizes perturbative predictions. We also observe from Fig. 4 that the  $\mu_\Gamma$  dependence of the peak-position is not reduced in going from LL, to NLL, to NNLL in the pole-scheme. However, in the jet-mass scheme the peak location converges nicely from LL to NLL to NNLL, with a numerical value of  $M_t^{\text{peak}} = 172.099$  GeV at NNLL order. At  $\mu_\Gamma = 5$  GeV the shifts are  $\simeq 67$  MeV from LL to NLL and  $\simeq 17$  MeV from NLL to NNLL. Also in the jet-scheme, Fig. 4 shows that the  $\mu_\Gamma$  dependence of the peak-position decreases from LL, to NLL, to NNLL order, with the curves becoming flatter as the order increases. The residual  $\mu_\Gamma$  scale dependence of the peak position in the jet-scheme is  $\delta M_t^{\text{peak}} = 0.005$  GeV, where we quote the difference in  $M_t^{\text{peak}}$  from  $\mu_\Gamma = 3$  GeV to  $\mu_\Gamma = 10$  GeV.

Utilizing the two-loop computation with NNLL renormalization group improvement, and a jet-mass scheme with good renormalization group behavior, we have achieved stable results for the heavy quark jet function. However, we caution that the final result for the jet function is dependent on the choice of  $\mu_\Lambda$ , and so a more detailed phenomenological analysis must be made only after combining the results reported here with perturbative corrections in the soft function to yield a  $\mu_\Lambda$  independent prediction for the cross-section. In particular the size of the perturbative tail above the peak in the cross-section is affected by both perturbative corrections to the jet function and soft-function, and is strongly  $\mu_\Lambda$  dependent in each of these functions individually.

## VII. CONCLUSION

Effective field theories are an important tool for making high precision predictions for jet observables, and facilitate a measurement of the top mass with theoretical uncertainty less than  $\mathcal{O}(\Lambda_{\text{QCD}})$ . Starting from the expression for the cross section for double top production at an  $e^+e^-$  collider, Eq. (2) derived in Ref. [12], we have studied the properties of the heavy-quark jet function  $B$  at higher loop orders. The function  $B$  can be calculated in HQET, and was studied at one-loop and NLL order in Ref. [19]. Here we have performed the 2-loop computation of  $B$  to obtain a NNLO result. Our analysis also yielded the two-loop anomalous dimension of  $B$ , which when combined with the three-loop cusp anomalous dimension from Ref. [61] was used to obtain a renormalization group improved heavy quark jet function at NNLL order. Using the formulation in terms of vacuum matrix elements of Wilson lines we have explained precisely how the jet function is different from the heavy-quark shape function and fragmentation function that have been considered previously in the literature at two-loop order [38, 39, 40, 41].

The two-loop computation also allowed us to study the higher loop behavior of  $B$  and arrive at a suitable definition of a short distance top mass-scheme, for higher order analysis. In particular we gave a definition for a jet-mass scheme with nice renormalization group properties, and demonstrated that in this scheme the mass anomalous dimension is determined by the cusp anomalous dimension to all orders in perturbation theory. To study the properties of different mass-scheme definitions we exploited the fact that the heavy-quark jet function in position space fulfills the requirements to obey the non-abelian exponentiation theorem of Refs. [36, 37]. In particular in the abelian limit ( $C_A, n_f \rightarrow 0$ ) the all orders result for  $B$  is simply the exponentiated one-loop result. We considered differences between a peak-position mass definition, a first moment mass definition, and a mass definition based on the position space jet function. We have checked that among these three possibilities, the peak definition and moment definition do not yield consistent mass renormalization group equations at LO and NLO order respectively. Thus only the position space definition provides a reasonable way of defining the jet-mass beyond LL order. This definition is given in Eq. (57)c. Relations between the jet-mass and the  $\overline{\text{MS}}$ , 1S, and pole masses were also given at two-loop order. The proof that the jet-mass is a short-distance mass, free from leading order renormalon ambiguities, is given in Ref. [65].

Our final result for the heavy-quark jet function  $B$  uses the jet-mass scheme with NNLO fixed order results and a NNLL resummation of large logarithms, which we refer to as the NNLL order result. The logs in this summation are a well defined set for a physical observable, being the only large logs that effect the shape of the top-invariant mass cross-section  $d^2\sigma/dM_t^2 dM_{\bar{t}}^2$ . We have studied the numerical stability of  $B$ , both in terms of perturbative convergence from LL, to NLL, to NNLL order, and with respect to its scale dependence. In the jet-mass scheme the convergence of  $B$  improves by a factor of two or better in going from NLL to NNLL order. Very stable results were also obtained for the peak position of the heavy-quark jet function, with residual perturbative uncertainties estimated to be at the 5 MeV level. This level of precision and stability for the jet function and its peak-position were not observed in the pole-mass scheme.

Future applications of our work include the extension to complete NNLL results for the cross-section  $d^2\sigma/dM_t^2 dM_{\bar{t}}^2$  by including the convolution with the soft-function and its perturbative and non-perturbative components. The use of position space as a convenient way of defining a top mass-scheme, could also be extended to the b-quark where currently a moment mass scheme, called the shape-function scheme [9], is often employed. Based on our analysis we expect that this shape function mass also does not have a consistent anomalous dimension beyond LL order, but that this can be rectified by using a modified definition of the scheme in position space. Finally, the same position space technique can be applied to the definition of the renormalon free gap parameter [22], a parameter which is important

for combining perturbative and non-perturbative results for the soft-function for jet production.

### Acknowledgments

We would like to thank A. Hoang for helpful comments. This work was supported in part by the Department of Energy Office of Nuclear Science under the grant DE-FG02-94ER40818. I. Scimemi was also supported in part by a Marie Curie International Fellowship from the European Union, grant number 021379 (BDECMIT), and thanks the Fundació Bosch i Gimpera and J. Soto of the University of Barcelona (Spain) for support. I.W. Stewart was also supported in part by the DOE Outstanding Junior Investigator program and Sloan Foundation.

### APPENDIX A: TWO-LOOP GRAPHS AND RENORMALIZATION

In this section we briefly summarize results for the two-loop jet function graphs and their renormalization factors. We use Feynman gauge and dimensional regularization with  $d = 4 - 2\epsilon$ . Numbering the two-loop graphs in Fig. 1 from left-to-right and top-to-bottom we have

$$\iota^{2\epsilon} \mu^{4\epsilon} \mathcal{B}_2^{\text{bare}}(\hat{s}) = \sum_{i=1}^{16} G_i, \quad G_i = \frac{i\alpha_s^2(\mu)}{4\pi^2 a} \hat{G}_i, \quad (\text{A1})$$

where we have defined  $\hat{G}_i$  by pulling out a common prefactor, and we let  $a = \hat{s} + i0$  and  $\iota = \exp(\gamma_E)/(4\pi)$ . The sum of terms for  $\mathcal{B}_2^{\text{bare}}$  is gauge invariant. In Feynman gauge the results for the  $\hat{G}_i$ 's in terms of master integrals are

$$\begin{aligned} \hat{G}_1 &= 4C_F T_F n_f h_{1\epsilon} + 4C_F^2 h_{2\epsilon} - C_F C_A h_{3\epsilon}, & \hat{G}_2 &= 8C_F^2 F_0(1, 1, 1)F_0(1, 1, 0) \\ \hat{G}_3 &= 2C_F^2 [F_0(1, 1, 1)]^2, & \hat{G}_4 &= -8C_F^2 F(101, 210, 100), \\ \hat{G}_5 &= -8C_F \left(C_F - \frac{1}{2}C_A\right) F(101, 111, 100), & \hat{G}_6 &= -2C_F \left(C_F - \frac{1}{2}C_A\right) F(101, 111, 101), \\ \hat{G}_7 &= C_F C_A [F(111, 100, 010) - 2F(111, 100, 100) + 4F(111, 110, 10-1) + 2F(111, 110, 000) + F(111, 110, 100)], \\ \hat{G}_8 &= C_F C_A F(111, 110, 100), & \hat{G}_9 &= -4C_F^2 F(101, 110, 101) + 2C_F C_A F(101, 110, 011), \\ \hat{G}_{10} &= -C_F C_A [2F(111, 010, 010) - F(111, 010, 100)], \\ \hat{G}_{11} &= (4C_F T_F n_f f_{1\epsilon} - 2C_F C_A f_{2\epsilon}) [2F_0(1 + \epsilon, 1, 1) + F_0(2 + \epsilon, 1, 0)], \\ \hat{G}_{12} &= (-2C_F T_F n_f f_{1\epsilon} + C_F C_A f_{2\epsilon}) F_0(2 + \epsilon, 1, 0), & \hat{G}_{13} &= \hat{G}_{14} = \hat{G}_{15} = \hat{G}_{16} = 0. \end{aligned} \quad (\text{A2})$$

Here  $T_F = 1/2$ ,  $C_A = 3$ ,  $C_F = 4/3$ . The  $\hat{G}_1$  and the  $h_{i\epsilon}$  are determined by the two-loop computation of the heavy-quark self-energy in Ref. [59, 60], while the  $f_{i\epsilon}$  are determined from the standard sum of one-loop quark, ghost, and gluon vacuum polarization graphs. We have

$$\begin{aligned} f_{1\epsilon} &= \left(\frac{\mu}{-a}\right)^{2\epsilon} \frac{(1-\epsilon) e^{\epsilon\gamma_E} (-1)^{1+\epsilon} \Gamma^2(1-\epsilon)\Gamma(1+\epsilon)}{\epsilon(3-2\epsilon)(1-2\epsilon) \Gamma(1-2\epsilon)}, & f_{2\epsilon} &= \left(\frac{\mu}{-a}\right)^{2\epsilon} \frac{(5-3\epsilon) e^{\epsilon\gamma_E} (-1)^{1+\epsilon} \Gamma^2(1-\epsilon)\Gamma(1+\epsilon)}{2\epsilon(3-2\epsilon)(1-2\epsilon) \Gamma(1-2\epsilon)}, \\ h_{1\epsilon} &= \left(\frac{\mu}{-a}\right)^{4\epsilon} \frac{(1-\epsilon)\Gamma^2(1-\epsilon)\Gamma(1+4\epsilon)e^{2\epsilon\gamma_E}}{2\epsilon^2(1-2\epsilon)(-2-2\epsilon)(1-4\epsilon)}, & h_{2\epsilon} &= \left(\frac{\mu}{-a}\right)^{4\epsilon} \frac{\Gamma^2(1-\epsilon)\Gamma(1+4\epsilon)e^{2\epsilon\gamma_E}}{4\epsilon^2(1-2\epsilon)^2}, \\ h_{3\epsilon} &= -\left(\frac{\mu}{-a}\right)^{4\epsilon} \frac{\Gamma^2(1-\epsilon)e^{2\epsilon\gamma_E}}{4\epsilon^2(1+\epsilon)(1-4\epsilon)(1-2\epsilon)^2} \left[ (10\epsilon^2 - 9\epsilon + 5) \Gamma(1+4\epsilon) + 4(1+\epsilon)(1-4\epsilon)\Gamma^2(1+2\epsilon) \right]. \end{aligned} \quad (\text{A3})$$

The results in Eq. (A2) are given in terms of the one-loop master integral

$$F_0(\lambda_1 \lambda_2 \lambda_3) \equiv -iN_d \int \frac{d^d \ell}{(2\pi)^d} \frac{a^{-4+2\lambda_1+\lambda_2+\lambda_3} (\bar{n} \cdot v)^{\lambda_3}}{[\ell^2]^{\lambda_1} [2v \cdot \ell + a]^{\lambda_2} [\bar{n} \cdot \ell]^{\lambda_3}} = (-1)^{4-\lambda_1} \left(\frac{\mu}{-a}\right)^{2\epsilon} \frac{e^{\epsilon\gamma_E} \Gamma(2\lambda_1 + \lambda_2 + \lambda_3 - d) \Gamma(d/2 - \lambda_1 - \lambda_3)}{\Gamma(\lambda_1)\Gamma(\lambda_2)}, \quad (\text{A4})$$

where  $N_d = (4\pi)^{d/2} \mu^{2\epsilon} e^{\gamma_E \epsilon}$ , and the two-loop master integral

$$\begin{aligned} &F(\lambda_1 \lambda_2 \lambda_3, \lambda_4 \lambda_5 \lambda_6, \lambda_7 \lambda_8 \lambda_9) \\ &\equiv \int \frac{d^d \ell d^d k}{(2\pi)^{2d}} \frac{N_d^2 a^{(2\lambda_1+2\lambda_2+2\lambda_3+\lambda_4+\lambda_5+\lambda_6+\lambda_7+\lambda_8+\lambda_9-8)} [\bar{n} \cdot v]^{(\lambda_7+\lambda_8+\lambda_9)}}{[\ell^2]^{\lambda_1} [(\ell+k)^2]^{\lambda_2} [k^2]^{\lambda_3} [2v \cdot \ell + a]^{\lambda_4} [2v \cdot (\ell+k) + a]^{\lambda_5} [2v \cdot k + a]^{\lambda_6} [\bar{n} \cdot \ell]^{\lambda_7} [\bar{n} \cdot \ell + \bar{n} \cdot k]^{\lambda_8} [\bar{n} \cdot k]^{\lambda_9}}. \end{aligned} \quad (\text{A5})$$

All denominator factors in square brackets in Eq. (A4) and (A5) have  $+i0$ . As written, in the light-like propagators  $[\bar{n} \cdot k]$ ,  $[\bar{n} \cdot l + \bar{n} \cdot k]$ ,  $[\bar{n} \cdot k]$  this prescription for  $+i0$ 's does not precisely match the  $i0$ 's from the definition in Eq. (44). However we have checked that the difference results in scaleless integrals which are cancelled by 0-bin subtraction terms [45], which are part of the definition of propagators of the collinear fields in the jet function [12]. All 0-bin subtraction terms are also scaleless and therefore have not been shown explicitly. For the heavy quark jet function the result of adding these contributions is simply that the  $1/\epsilon$  divergences from the integrals in Eq. (A2) are all UV. The general result for  $F(\lambda_1 \lambda_2 \lambda_3, \lambda_4 \lambda_5 \lambda_6, \lambda_7 \lambda_8 \lambda_9)$  is not known. Several of these master integrals could be obtained from the calculation in Ref. [40] by shifts of variable that move  $a$  into the light-like denominators, but these are not the integrals needed for our analysis. We have therefore computed the master integral for the cases appearing in Eq. (A2). Two cases are iterations of the one-loop master integral,  $F(101, 110, 101) = -F_0(1, 1 + 2\epsilon, 1)F_0(1, 1, 1)$  and  $F(101, 210, 100) = -F_0(1, 1 + 2\epsilon, 1)F_0(1, 1, 0)$ . In order to evaluate some of the remaining cases we have used the integration by parts technique [70, 71]. For simplicity we quote the results as series in  $\epsilon$ ,

$$\begin{aligned}
F(101, 110, 011) &= \left(\frac{\mu}{-a}\right)^{4\epsilon} \left(-\frac{1}{8\epsilon^4} - \frac{11\pi^2}{48\epsilon^2} + \frac{17\zeta_3}{6\epsilon} - \frac{907\pi^4}{2880}\right), \\
F(101, 111, 100) &= \left(\frac{\mu}{-a}\right)^{4\epsilon} \left(\frac{1}{8\epsilon^3} + \frac{1}{4\epsilon^2} + \frac{1}{2\epsilon} + \frac{\pi^2}{48\epsilon} + \frac{17\zeta_3}{12} + \frac{\pi^2}{24} + 1\right), \\
F(101, 111, 101) &= \left(\frac{\mu}{-a}\right)^{4\epsilon} \left(-\frac{\pi^2}{6\epsilon^2} + \frac{4\zeta_3}{\epsilon} - \frac{7\pi^4}{20}\right), \\
F(111, 100, 010) &= \left(\frac{\mu}{-a}\right)^{4\epsilon} \left(\frac{1}{8\epsilon^4} + \frac{3\pi^2}{16\epsilon^2} - \frac{31\zeta_3}{12\epsilon} + \frac{221\pi^4}{960}\right), \\
F(111, 100, 100) &= \left(\frac{\mu}{-a}\right)^{4\epsilon} \left(-\frac{1}{8\epsilon^3} - \frac{1}{4\epsilon^2} - \frac{3\pi^2}{16\epsilon} - \frac{1}{2\epsilon} + \frac{31\zeta_3}{12} - \frac{3\pi^2}{8} - 1\right), \\
F(111, 110, 000) &= \left(\frac{\mu}{-a}\right)^{4\epsilon} \left(\frac{\pi^2}{6\epsilon} - 4\zeta_3 + \frac{\pi^2}{3}\right), \\
F(111, 110, 100) &= \left(\frac{\mu}{-a}\right)^{4\epsilon} \left(\frac{\pi^2}{12\epsilon^2} - \frac{7\zeta_3}{2\epsilon} + \frac{13\pi^4}{72}\right), \\
F(111, 110, 10-1) &= \left(\frac{\mu}{-a}\right)^{4\epsilon} \left(-\frac{1}{8\epsilon^3} - \frac{1}{4\epsilon^2} - \frac{7\pi^2}{48\epsilon} - \frac{1}{2\epsilon} - \frac{2\zeta_3}{3} + \frac{\pi^2}{24} - 1\right). \tag{A6}
\end{aligned}$$

To determine the counterterms  $\bar{Z}_i^{(j)}$  we use the analog of Eq. (34) where we set  $\delta m = 0$  and take the imaginary part of both sides. Since  $\text{Im}[m\mathcal{B}_0(\hat{s}, \mu)] = \delta(\hat{s})$  this gives a simpler set of equations for the terms in the renormalized jet function. At one-loop we have  $mB_1(\hat{s}, \mu) = \bar{Z}_1(\hat{s}, \mu) + \iota^\epsilon \mu^{2\epsilon} mB_1^{\text{bare}}(\hat{s})$ , and at two-loops

$$mB_2(\hat{s}, \mu) = \bar{Z}_2(\hat{s}, \mu) + \iota^{2\epsilon} \mu^{4\epsilon} mB_2^{\text{bare}}(\hat{s}) + 2z_{g1} \iota^\epsilon \mu^{2\epsilon} mB_1^{\text{bare}}(\hat{s}) + \int d\hat{s}' \bar{Z}_1(\hat{s} - \hat{s}', \mu) \iota^\epsilon \mu^{2\epsilon} mB_1^{\text{bare}}(\hat{s}'). \tag{A7}$$

Here  $z_{g1} = -\beta_0/8$  enters from coupling constant renormalization. To evaluate the convolution integral term in Eq. (A7) we need  $B_1^{\text{bare}}$  up to  $\mathcal{O}(\epsilon^2)$ , so the required ingredients from one-loop graphs are

$$\begin{aligned}
\iota^\epsilon \mu^{2\epsilon} mB_1^{\text{bare}}(\hat{s}) &= C_F \left[ \frac{4\epsilon^2}{3} \mathcal{L}^3 - (2\epsilon + 2\epsilon^2) \mathcal{L}^2 + \left(2 + 2\epsilon + 4\epsilon^2 - \frac{\pi^2}{2}\epsilon^2\right) \mathcal{L}^1 - \left(\frac{1}{\epsilon} + 1 + 2\epsilon - \frac{\pi^2}{4}\epsilon - \frac{7\zeta_3}{3}\epsilon^2 - \frac{\pi^2}{4}\epsilon^2 + 4\epsilon^2\right) \mathcal{L}^0 \right. \\
&\quad \left. + \left(\frac{1}{2\epsilon^2} + \frac{1}{2\epsilon} + 1 - \frac{\pi^2}{8} + 2\epsilon - \frac{\pi^2}{8}\epsilon - \frac{7\zeta_3}{6}\epsilon - \frac{7\zeta_3}{6}\epsilon^2 - \frac{\pi^4}{192}\epsilon^2 - \frac{\pi^2}{4}\epsilon^2 + 4\epsilon^2\right) \delta(\hat{s}) \right] + \mathcal{O}(\epsilon^3), \\
\bar{Z}_1(\hat{s}, \mu) &= C_F \left[ \frac{1}{\epsilon} \mathcal{L}^0 - \left(\frac{1}{2\epsilon^2} + \frac{1}{2\epsilon}\right) \delta(\hat{s}) \right], \tag{A8}
\end{aligned}$$

where the distribution  $\mathcal{L}^k$  was defined in Eq. (40). From Eq. (A1) the sum of the two-loop graphs gives

$$\begin{aligned}
\iota^{2\epsilon} \mu^{4\epsilon} m B_2^{\text{bare}}(\hat{s}) &= C_F C_A \left\{ \left( \frac{2}{3} - \frac{\pi^2}{6} \right) \mathcal{L}^1 - \left( \frac{1}{6\epsilon} - \frac{\pi^2}{24\epsilon} + \frac{5}{18} - \frac{\pi^2}{12} - \frac{5\zeta_3}{4} \right) \mathcal{L}^0 \right. \\
&\quad \left. + \left( \frac{1}{24\epsilon^2} - \frac{\pi^2}{96\epsilon^2} + \frac{5}{72\epsilon} - \frac{\pi^2}{48\epsilon} - \frac{5\zeta_3}{16\epsilon} - \frac{11}{54} - \frac{\pi^2}{144} + \frac{23\pi^4}{2880} - \frac{5\zeta_3}{8} \right) \delta(\hat{s}) \right\} \\
&+ C_F^2 \left\{ \frac{16}{3} \mathcal{L}^3 - \left( 8 + \frac{4}{\epsilon} \right) \mathcal{L}^2 + \left( \frac{2}{\epsilon^2} + \frac{4}{\epsilon} + 10 - \frac{7\pi^2}{3} \right) \mathcal{L}^1 - \left( \frac{1}{2\epsilon^3} + \frac{1}{\epsilon^2} + \frac{5}{2\epsilon} - \frac{7\pi^2}{12\epsilon} - \frac{31\zeta_3}{3} - \frac{7\pi^2}{6} + 6 \right) \mathcal{L}^0 \right. \\
&\quad \left. + \left( \frac{1}{8\epsilon^4} + \frac{1}{4\epsilon^3} + \frac{5}{8\epsilon^2} - \frac{7\pi^2}{48\epsilon^2} + \frac{3}{2\epsilon} - \frac{7\pi^2}{24\epsilon} - \frac{31\zeta_3}{12\epsilon} + \frac{7}{2} - \frac{35\pi^2}{48} - \frac{\pi^4}{320} - \frac{31\zeta_3}{6} \right) \delta(\hat{s}) \right\} \\
&+ C_F \beta_0 \left\{ -\mathcal{L}^2 + \left( \frac{1}{2\epsilon} + \frac{11}{6} \right) \mathcal{L}^1 - \left( \frac{1}{8\epsilon^2} + \frac{11}{24\epsilon} + \frac{65}{36} - \frac{7\pi^2}{48} \right) \mathcal{L}^0 \right. \\
&\quad \left. + \left( \frac{1}{32\epsilon^3} + \frac{11}{96\epsilon^2} + \frac{65}{144\epsilon} - \frac{7\pi^2}{192\epsilon} + \frac{389}{216} - \frac{77\pi^2}{576} - \frac{31\zeta_3}{48} \right) \delta(\hat{s}) \right\} + \mathcal{O}(\epsilon). \tag{A9}
\end{aligned}$$

The convolution integral required in Eq. (A7) is given by

$$\begin{aligned}
&\int d\hat{s}' \bar{Z}_1(\hat{s} - \hat{s}', \mu) \iota^\epsilon \mu^{2\epsilon} m B_1^{\text{bare}}(\hat{s}') \\
&= C_F^2 \left\{ -\frac{10}{3} \mathcal{L}^3 + \left( \frac{4}{\epsilon} + 5 \right) \mathcal{L}^2 - \left( \frac{3}{\epsilon^2} + \frac{4}{\epsilon} + 7 - \frac{17\pi^2}{12} \right) \mathcal{L}^1 + \left( \frac{1}{\epsilon^3} + \frac{3}{2\epsilon^2} + \frac{5}{2\epsilon} - \frac{7\pi^2}{12\epsilon} + 5 - \frac{17\pi^2}{24} - \frac{19\zeta_3}{3} \right) \mathcal{L}^0 \right. \\
&\quad \left. - \left( \frac{1}{4\epsilon^4} + \frac{1}{2\epsilon^3} + \frac{3}{4\epsilon^2} - \frac{11\pi^2}{48\epsilon^2} + \frac{3}{2\epsilon} - \frac{7\pi^2}{24\epsilon} - \frac{31\zeta_3}{12\epsilon} + 3 - \frac{25\pi^2}{48} - \frac{31\pi^4}{5760} - \frac{19\zeta_3}{6} \right) \delta(\hat{s}) \right\}. \tag{A10}
\end{aligned}$$

In order to obtain this result we have used Eq. (A8) along with Eq. (B7) from Appendix B. Combining the last three terms in Eq. (A7) the remaining  $1/\epsilon^k$  terms must be canceled by  $\bar{Z}_2$ , hence uniquely fixing it. This gives

$$\begin{aligned}
\tilde{Z}_2(\hat{s}) &= C_F^2 \left\{ \frac{1}{\epsilon^2} \mathcal{L}^1 - \left( \frac{1}{2\epsilon^3} + \frac{1}{2\epsilon^2} \right) \mathcal{L}^0 + \left( \frac{1}{8\epsilon^4} + \frac{1}{4\epsilon^3} + \frac{1}{8\epsilon^2} - \frac{\pi^2}{12\epsilon^2} \right) \delta(\hat{s}) \right\} \\
&\quad + C_F C_A \left\{ \left( \frac{1}{6\epsilon} - \frac{\pi^2}{24\epsilon} \right) \mathcal{L}^0 + \left( -\frac{1}{24\epsilon^2} + \frac{\pi^2}{96\epsilon^2} - \frac{5}{72\epsilon} + \frac{\pi^2}{48\epsilon} + \frac{5\zeta_3}{16\epsilon} \right) \delta(\hat{s}) \right\} \\
&\quad + C_F \beta_0 \left\{ \left( -\frac{1}{8\epsilon^2} + \frac{5}{24\epsilon} \right) \mathcal{L}^0 + \left( \frac{3}{32\epsilon^3} + \frac{1}{96\epsilon^2} - \frac{29}{144\epsilon} + \frac{\pi^2}{192\epsilon} \right) \delta(\hat{s}) \right\}. \tag{A11}
\end{aligned}$$

Using the notation in Eq. (35) the counterterm consistency equations that follow from Eq. (22) are

$$\begin{aligned}
\mu \frac{\partial}{\partial \mu} \bar{Z}_1^{(1)} &= 2\bar{Z}_1^{(2)}, & \mu \frac{\partial}{\partial \mu} \bar{Z}_1^{(2)} &= 0, & \mu \frac{\partial}{\partial \mu} \bar{Z}_2^{(3)} &= 4\bar{Z}_2^{(4)}, \\
4\bar{Z}_2^{(3)} &= \mu \frac{\partial}{\partial \mu} \bar{Z}_2^{(2)} - \frac{\beta_0}{2} \bar{Z}_1^{(2)} + 2 \int d\hat{s}' \bar{Z}_1^{(2)}(\hat{s} - \hat{s}', \mu) \bar{Z}_1^{(1)}(\hat{s}'), \\
4\bar{Z}_2^{(2)} &= \mu \frac{\partial}{\partial \mu} \bar{Z}_2^{(1)} - \frac{\beta_0}{2} \bar{Z}_1^{(1)} + 2 \int d\hat{s}' \bar{Z}_1^{(1)}(\hat{s} - \hat{s}', \mu) \bar{Z}_1^{(1)}(\hat{s}'). \tag{A12}
\end{aligned}$$

Reading off the coefficients of various powers of  $1/\epsilon^k$  from the results in Eqs. (A8) and (A11) we can verify that they are all satisfied.

## APPENDIX B: RELATIONS FOR PLUS-DISTRIBUTIONS

In the text in several places we converted between momentum space, position space, and plus-distributions arising from imaginary parts. Useful conversion formulas include

$$\text{FT}[\ln^k(i y \mu e^{\gamma_E})] = \frac{d^k}{d\epsilon^k} \frac{e^{\epsilon \gamma_E}}{\Gamma(1-\epsilon)} \left\{ \delta(\hat{s}) - \frac{\epsilon}{\mu} \left[ \frac{\theta(\hat{s}) e^{-\epsilon \ln(\hat{s}/\mu)}}{\hat{s}/\mu} \right]_+ \right\} \Big|_{\epsilon=0}. \tag{B1}$$

and

$$\text{Im} \left[ \frac{\ln^n(-x-i0)}{\pi(-x-i0)} \right] = \cos^2 \left( \frac{n\pi}{2} \right) \frac{(-\pi^2)^{n/2}}{n+1} \delta(x) + \sum_{j=0}^{\lfloor \frac{n-1}{2} \rfloor} \frac{(-1)^j n! \pi^{2j}}{(2j+1)!(n-2j-1)!} \left[ \frac{\theta(x) \ln^{n-2j-1}(x)}{x} \right]_+, \quad (\text{B2})$$

where  $\lfloor p \rfloor$  on the sum is the greatest integer not exceeding  $p$ . From Eq. (B2) the cases we used include

$$\begin{aligned} \text{Im}[L^0] &= \delta(\hat{s}), & \text{Im}[L^1] &= -\mathcal{L}^0, & \text{Im}[L^2] &= 2\mathcal{L}^1 - \frac{\pi^2}{3}\delta(\hat{s}), \\ \text{Im}[L^3] &= -3\mathcal{L}^2 + \pi^2\mathcal{L}^0, & \text{Im}[L^4] &= 4\mathcal{L}^3 - 4\pi^2\mathcal{L}^1 + \frac{\pi^4}{5}\delta(\hat{s}), & \text{Im}[L^5] &= -5\mathcal{L}^4 + 10\pi^2\mathcal{L}^2 - \pi^4\mathcal{L}^0, \\ \text{Im}[L^6] &= 6\mathcal{L}^5 - 20\pi^2\mathcal{L}^3 + 6\pi^4\mathcal{L}^1 - \frac{\pi^6}{7}\delta(\hat{s}). \end{aligned} \quad (\text{B3})$$

Here  $L^k$  is defined by Eq. (37) and the distribution  $\mathcal{L}^k$  is defined in Eq. (40). The following rescaling identity is also useful

$$\frac{1}{\lambda} \left[ \frac{\lambda \theta(x) \log^p(x/\lambda)}{x} \right]_+ = \sum_{k=0}^p \frac{p!}{(p-k)!k!} \log^{p-k} \left( \frac{1}{\lambda} \right) \left[ \frac{\theta(x) \log^k x}{x} \right]_+ + \frac{\delta(x)}{(p+1)} \log^{p+1} \left( \frac{1}{\lambda} \right). \quad (\text{B4})$$

For  $k \geq 0$  this result readily gives

$$\mu \frac{d}{d\mu} \mathcal{L}^k = -k\mathcal{L}^{k-1} - \delta_{k,0} \delta(\hat{s}). \quad (\text{B5})$$

Eq. (B5) can be used to verify the expected  $\mu$ -dependence at various stages. Finally, we need the convolution of two plus distributions. The general formula is

$$\begin{aligned} \int d\hat{s}' \mathcal{L}^j(\hat{s} - \hat{s}') \mathcal{L}^k(\hat{s}') &= \delta(\hat{s}) (-1)^{k+j} \frac{d^k}{dw'^k} \frac{d^j}{dw^j} \left\{ \frac{\Gamma(-w)\Gamma(-w')}{\Gamma(1-w-w')} - \frac{1}{ww'} \right\} \Big|_{w=w'=0} \\ &+ \frac{1}{\mu} \left[ (-1)^{k+j} \frac{d^k}{dw'^k} \frac{d^j}{dw^j} \left( \frac{\hat{s}}{\mu} \right)^{-1-w-w'} \left\{ \frac{1}{w} + \frac{1}{w'} + \frac{\Gamma(-w)\Gamma(-w')}{\Gamma(-w-w')} \right\} \Big|_{w=w'=0} + \left( \frac{1}{k+1} + \frac{1}{j+1} \right) \frac{(\ln \hat{s}/\mu)^{k+j+1}}{\hat{s}/\mu} \right]_+. \end{aligned} \quad (\text{B6})$$

The following cases were used in our analysis

$$\begin{aligned} \int d\hat{s}' \mathcal{L}^0(\hat{s} - \hat{s}') \mathcal{L}^0(\hat{s}') &= 2\mathcal{L}^1(\hat{s}) - \frac{\pi^2}{6} \delta(\hat{s}), \\ \int d\hat{s}' \mathcal{L}^0(\hat{s} - \hat{s}') \mathcal{L}^1(\hat{s}') &= \frac{3}{2}\mathcal{L}^2(\hat{s}) - \frac{\pi^2}{6} \mathcal{L}^0 + \zeta_3 \delta(\hat{s}), \\ \int d\hat{s}' \mathcal{L}^0(\hat{s} - \hat{s}') \mathcal{L}^2(\hat{s}') &= \frac{4}{3}\mathcal{L}^3(\hat{s}) - \frac{\pi^2}{3} \mathcal{L}^1(\hat{s}) + 2\zeta_3 \mathcal{L}^0 - \frac{\pi^4}{45} \delta(\hat{s}). \end{aligned} \quad (\text{B7})$$

- 
- [1] Tevatron Electroweak Working Group (2007), hep-ex/0703034.  
[2] M. Gruenewald, EPS-HEP, Manchester, (2007), arXiv:0709.3744.  
[3] W. M. Yao et al. (Particle Data Group), J. Phys. **G33**, 1 (2006).  
[4] HFAG (Heavy Flavor Averaging Group) (2007).  
[5] I. I. Y. Bigi, M. A. Shifman, N. Uraltsev, and A. I. Vainshtein, Phys. Rev. **D56**, 4017 (1997), hep-ph/9704245.  
[6] A. H. Hoang, Z. Ligeti, and A. V. Manohar, Phys. Rev. **D59**, 074017 (1999), hep-ph/9811239.  
[7] A. H. Hoang, Z. Ligeti, and A. V. Manohar, Phys. Rev. Lett. **82**, 277 (1999), hep-ph/9809423.  
[8] A. H. Hoang and T. Teubner, Phys. Rev. **D60**, 114027 (1999), hep-ph/9904468.  
[9] S. W. Bosch, B. O. Lange, M. Neubert, and G. Paz, Nucl. Phys. **B699**, 335 (2004), hep-ph/0402094.  
[10] M. Beneke, Phys. Rept. **317**, 1 (1999), hep-ph/9807443.  
[11] M. C. Smith and S. S. Willenbrock, Phys. Rev. Lett. **79**, 3825 (1997), hep-ph/9612329.  
[12] S. Fleming, A. H. Hoang, S. Mantry, and I. W. Stewart, Phys. Rev. **D77**, 074010 (2008), hep-ph/0703207.



- [13] A. H. Hoang et al., Eur. Phys. J. direct **C2**, 1 (2000), hep-ph/0001286.
- [14] A. H. Hoang, A. V. Manohar, I. W. Stewart, and T. Teubner, Phys. Rev. **D65**, 014014 (2002), hep-ph/0107144.
- [15] A. Pineda and A. Signer, Nucl. Phys. **B762**, 67 (2007), hep-ph/0607239.
- [16] M. Martinez and R. Miquel, Eur. Phys. J. **C27**, 49 (2003), hep-ph/0207315.
- [17] A. Juste et al., ECONF C0508141, PLEN0043 (2005), hep-ph/0601112.
- [18] A. H. Hoang and C. J. Reisser, Phys. Rev. **D74**, 034002 (2006), hep-ph/0604104.
- [19] S. Fleming, A. H. Hoang, S. Mantry, and I. W. Stewart (2007), 0711.2079 [hep-ph].
- [20] A. V. Manohar and M. B. Wise, Camb. Monogr. Part. Phys. Nucl. Phys. Cosmol. **10**, 1 (2000).
- [21] M. Neubert, Phys. Rept. **245**, 259 (1994), hep-ph/9306320.
- [22] A. H. Hoang and I. W. Stewart, Phys. Lett. **B660**, 483 (2008), 0709.3519 [hep-ph].
- [23] G. P. Korchemsky and S. Tafat, JHEP **10**, 010 (2000), hep-ph/0007005.
- [24] C. W. Bauer, S. Fleming, and M. E. Luke, Phys. Rev. **D63**, 014006 (2000), hep-ph/0005275.
- [25] C. W. Bauer, S. Fleming, D. Pirjol, and I. W. Stewart, Phys. Rev. **D63**, 114020 (2001), hep-ph/0011336.
- [26] C. W. Bauer, D. Pirjol, and I. W. Stewart, Phys. Rev. **D65**, 054022 (2002), hep-ph/0109045.
- [27] C. W. Bauer and I. W. Stewart, Phys. Lett. **B516**, 134 (2001), hep-ph/0107001.
- [28] V. S. Fadin and V. A. Khoze, JETP Lett. **46**, 525 (1987).
- [29] M. Beneke, A. P. Chapovsky, A. Signer, and G. Zanderighi, Phys. Rev. Lett. **93**, 011602 (2004), hep-ph/0312331.
- [30] M. Beneke, A. P. Chapovsky, A. Signer, and G. Zanderighi, Nucl. Phys. **B686**, 205 (2004), hep-ph/0401002.
- [31] A. H. Hoang and C. J. Reisser, Phys. Rev. **D71**, 074022 (2005), hep-ph/0412258.
- [32] G. P. Korchemsky and G. Sterman, Nucl. Phys. **B437**, 415 (1995), hep-ph/9411211.
- [33] G. P. Korchemsky and G. Sterman, Nucl. Phys. **B555**, 335 (1999), hep-ph/9902341.
- [34] C. W. Bauer, A. V. Manohar, and M. B. Wise, Phys. Rev. Lett. **91**, 122001 (2003), hep-ph/0212255.
- [35] C. W. Bauer, C. Lee, A. V. Manohar, and M. B. Wise, Phys. Rev. **D70**, 034014 (2004), hep-ph/0309278.
- [36] J. G. M. Gatheral, Phys. Lett. **B133**, 90 (1983).
- [37] J. Frenkel and J. C. Taylor, Nucl. Phys. **B246**, 231 (1984).
- [38] G. P. Korchemsky and G. Marchesini, Nucl. Phys. **B406**, 225 (1993), hep-ph/9210281.
- [39] E. Gardi, JHEP **02**, 053 (2005), hep-ph/0501257.
- [40] T. Becher and M. Neubert, Phys. Lett. **B633**, 739 (2006), hep-ph/0512208.
- [41] M. Neubert (2007), arXiv:0706.2136 [hep-ph].
- [42] M. Neubert, Phys. Rev. **D49**, 3392 (1994), hep-ph/9311325.
- [43] I. I. Y. Bigi, M. A. Shifman, N. G. Uraltsev, and A. I. Vainshtein, Int. J. Mod. Phys. **A9**, 2467 (1994), hep-ph/9312359.
- [44] R. L. Jaffe and L. Randall, Nucl. Phys. **B412**, 79 (1994), hep-ph/9306201.
- [45] A. V. Manohar and I. W. Stewart, Phys. Rev. **D76**, 074002 (2007), hep-ph/0605001.
- [46] A. F. Falk, M. Neubert, and M. E. Luke, Nucl. Phys. **B388**, 363 (1992), hep-ph/9204229.
- [47] A. M. Polyakov, Phys. Lett. **B82**, 247 (1979).
- [48] V. S. Dotsenko and S. N. Vergeles, Nucl. Phys. **B169**, 527 (1980).
- [49] R. Brandt, F. Neri, and M. Sato, Phys. Rev. **D24**, 879 (1981).
- [50] G. P. Korchemsky and A. V. Radyushkin, Nucl. Phys. **B283**, 342 (1987).
- [51] C. Balzereit, T. Mannel, and W. Kilian, Phys. Rev. **D58**, 114029 (1998), hep-ph/9805297.
- [52] M. Neubert, Eur. Phys. J. C **40**, 165 (2005), hep-ph/0408179.
- [53] D. J. Gross and F. Wilczek, Phys. Rev. Lett. **30**, 1343 (1973).
- [54] H. D. Politzer, Phys. Rev. Lett. **30**, 1346 (1973).
- [55] D. R. T. Jones, Nucl. Phys. **B75**, 531 (1974).
- [56] W. E. Caswell, Phys. Rev. Lett. **33**, 244 (1974).
- [57] O. V. Tarasov, A. A. Vladimirov, and A. Y. Zharkov, Phys. Lett. **B93**, 429 (1980).
- [58] S. A. Larin and J. A. M. Vermaseren, Phys. Lett. **B303**, 334 (1993), hep-ph/9302208.
- [59] D. J. Broadhurst and A. G. Grozin, Phys. Lett. **B267**, 105 (1991), hep-ph/9908362.
- [60] A. G. Grozin (2000), hep-ph/0008300.
- [61] S. Moch, J. A. M. Vermaseren, and A. Vogt, Nucl. Phys. **B688**, 101 (2004), hep-ph/0403192.
- [62] G. P. Korchemsky and A. V. Radyushkin, Phys. Lett. **B279**, 359 (1992), hep-ph/9203222.
- [63] J. Chay, C. Kim, Y. G. Kim, and J.-P. Lee, Phys. Rev. **D71**, 056001 (2005), hep-ph/0412110.
- [64] C. M. Arnesen, J. Kundu, and I. W. Stewart, Phys. Rev. **D72**, 114002 (2005), hep-ph/0508214.
- [65] S. Fleming, A. H. Hoang, S. Mantry, and I. Stewart, in preparation (2008).
- [66] C. W. Bauer and A. V. Manohar, Phys. Rev. **D70**, 034024 (2004), hep-ph/0312109.
- [67] B. O. Lange and M. Neubert, Phys. Rev. Lett. **91**, 102001 (2003), hep-ph/0303082.
- [68] N. Gray, D. J. Broadhurst, W. Grafe, and K. Schilcher, Z. Phys. **C48**, 673 (1990).
- [69] J. Fleischer, F. Jegerlehner, O. V. Tarasov, and O. L. Veretin, Nucl. Phys. **B539**, 671 (1999), hep-ph/9803493.
- [70] F. V. Tkachov, Phys. Lett. **B100**, 65 (1981).
- [71] K. G. Chetyrkin and F. V. Tkachov, Nucl. Phys. **B192**, 159 (1981).